UNIVERSITY OF CALIFORNIA,

IRVINE

Viscoelastic Hydrogels from Physically Entangled Polyethylene Glycol: Synthesis and Rheological Characterization

THESIS

submitted in partial satisfaction of the requirements

for the degree of

MASTER OF SCIENCE

in Biomedical Engineering

by

Christopher Nguyen

Thesis Committee:
Associate Professor Ronke M Olabisi, Chair
Assistant Professor Daryl Preece
Assistant Professor Pim Oomen

2026

TABLE OF CONTENTS

LIST OF FIGURES

LIST OF TABLES

ACKNOWLEDGMENTS

Before all else, I would like to say thank you so very much to my family and friends. To my parents, thank you so much for all you have done for me throughout my masters journey. Without you guys, I wouldn't have pursued a higher education and I will not forget the sacrifices you two made for me, I love you two so much. I want to also thank my closest friends for keeping me company while I was working on homework or projects, it was much needed as those projects and assignments were very stressful and you took my mind off of them for a bit. As for the friends I made at UCI, thank you for making the process of being a masters student more enjoyable and not feel like a torture chamber. I hope we stay connected for as long as possible. To my girlfriend, thank you so much for showering me with love and care when I was worried that I wouldn't make it to becoming a masters student. You being there by my side helped so much and I can not thank you enough.

Now, I would like to express my deepest gratitude to my advisor, Dr. Olabisi. Thank you so much for always taking time out of your busy schedule to help me as well as respond to the various emails I sent you when I needed help with my project. Thank you for also bringing me in so smoothly into the lab. I never felt like I was alone throughout starting my thesis project and that was because of the team-work culture you built in your lab and I loved it. I hope I can still email you after my masters career ended for some life advice.

I would also like to thank the members of the Olabisi Lab for also making my experience at UCI so much better. Thank you Rabab for being by my side when I was figuring out how to use the rheometer for the first time. Thank you Kate for shooting ideas to me while talking about my thesis project, and Thank you Annie for all the conversations we had throughout my time working in the lab. I will never forget any of you guys and I hope to stay in touch with you all.

ABSTRACT OF THE THESIS

Viscoelastic Hydrogels from Physically Entangled Polyethylene Glycol: Synthesis and Rheological Characterization

by

Christopher Nguyen

Master of Science in Biomedical Engineering

University of California, Irvine, 2026

Associate Professor Ronke M Olabisi, Chair

Age-related macular degeneration (AMD) is a leading cause of severe vision loss in the elderly and one of the major contributors to this disease is the structural and functional breakdown of the Bruch's membrane, and because of this, retinal pigment epithelial (RPE) cells degenerate shortly after. The Bruch's membrane is viscoelastic in nature and RPE cells are sensitive to those mechanical cues, therefore scaffolds that replicate this behavior may better support RPE health than purely elastic counterparts. Polyethylene glycol (PEG) offers an adjustable, biologically inert platform for this need, however most methods for implementing viscoelasticity into PEG hydrogels rely on complex reactions. This thesis presents a viscoelastic PEG hydrogel made by combining PEG-propionaldehyde and PEG-amine (5 kDa each), which then crosslinks through dynamic imine bonds while also going through physical chain entanglement during gelation. Elastic PEG diacrylate (PEGDA) hydrogels served as controls. Rheology test were performed on these hydrogels and it showed that PEGDA had a frequency independent modulus with no cross over between the G' and G" values, while the PEG-propionaldehyde/ PEG-amine hydrogel displayed a clear crossover at approximately 0.3-0.5 rad/s, confirming viscoelasticity. Degradation tests were also performed and it showed that hydrogel stability depends on network maturity. This work overall serves as a simplified technique for producing viscoelastic PEG scaffolds for cells requiring a viscoelastic environment, such as RPE cells.

CHAPTER 1. Introduction

1.1. The Etiology of Age Related Macular Degeneration

As the human body grows old, cellular function slowly declines, resulting in diminished regenerative capacity and increased vulnerability to degenerative diseases. Age related macular degeneration (AMD) is an example of this and is the leading cause of severe vision loss in individuals over the age of 55 [1,9,23]. AMD impairs vision by damaging the retina, which is a layer of neural tissue located in the back of the eye. The retina converts light into neural signals and any damage to this structure will lead to impaired vision. Because the macula is where central vision occurs, common symptoms of AMD are a central black spot and/or increased blurriness [1] (Figure 1.1).

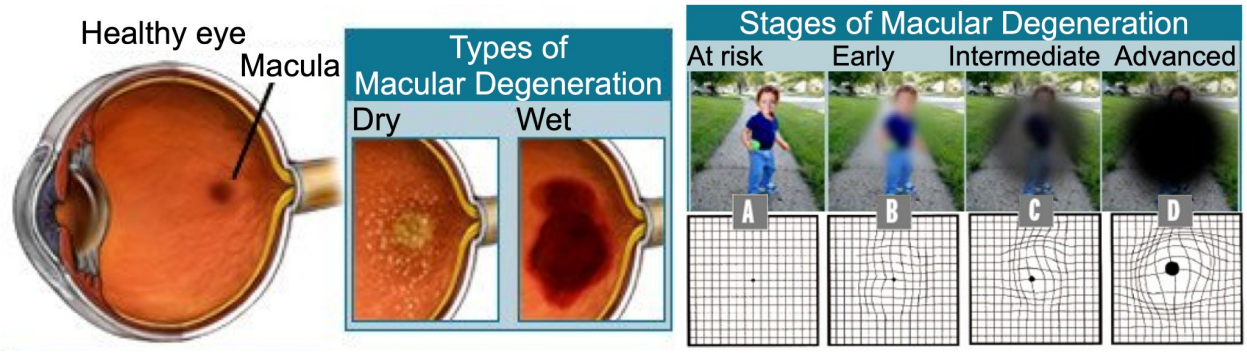

Figure 1.1 - The progression of AMD. Left image: A healthy eye. At the back of the eye, within the retina, is the macula, which is responsible for vision. Middle panel: macular degeneration is characterized as dry or wet, which describes how the damage is done to the retina. Right panel: As macular degeneration progresses, central vision also degenerates. [80]

The eye is composed of several layers (Figure 1.2). The sclera provides structural integrity, while the underlying choroid supplies oxygen and nutrients to the outer retina. The Bruch's membrane is situated between the choroid and the retinal pigment epithelium (RPE), regulating nutrient and waste exchange between the RPE and the choriocapillaris. RPE cells form a monolayer of specialized cells that are located between the photoreceptors of the retina and the Bruch's membrane (BM), which is a thin extracellular matrix (ECM) that separates the retina from the underlying choroidal blood supply [7,18]. The RPE supports photoreceptor health by recycling visual pigments, which are light-sensitive molecules found in the specialized outer segments of photoreceptor cells (rods and cones) in the retina [29]. The

RPE also phagocytoses shed outer segments and forms a blood-retinal barrier that regulates the transport of nutrients, water, and molecular solutes between the retina and choroid, while also preventing the infiltration of new blood vessels from the choroid [18,29]. In a healthy state, the Bruch's membrane serves as a selectively permeable barrier that facilitates the bidirectional transport of nutrients, oxygen, and waste products between the RPE and the choriocapillaris, the innermost layer of the choroidal vasculature [7]. Its structured composition of collagen and elastin layers provides mechanical support to the RPE while maintaining the integrity of the blood-retinal barrier, ensuring that the RPE can efficiently carry out its metabolic functions [7]. This positioning allows the RPE to extract nutrients from the blood and deliver them to the photoreceptors, while simultaneously collecting their waste products. Photoreceptors, comprising rods for low-light vision and cones for color and high-acuity central vision, transmit signals via bipolar and ganglion cells to the brain through the optic nerve [22]. The macula and fovea, densely populated with cone photoreceptors, are responsible for fine central vision. The macula is a dark spot at the center of the retina, which contains the fovea at its center. The fovea measures approximately 1.5 mm in diameter and contains the highest concentration of cone photoreceptor cells, which are essential for color vision and fine-tuned visual tasks such as reading, watching television, and recognizing faces [22]. These cells are among the most metabolically active cells in the entire body and require a large nutrient supply while producing a large amount of waste [3]. Because the light-absorbing components of photoreceptor cells must be replaced daily, the RPE acts as a recycling station, phagocytosing debris and releasing certain waste products into the bloodstream while recycling functional proteins and other useful materials for reuse [10,29]. In a healthy eye, this process ensures that no debris accumulates beneath the retina. In macular degeneration, progressive dysfunction of the RPE and Bruch's membrane leads to photoreceptor degeneration and irreversible central vision loss.

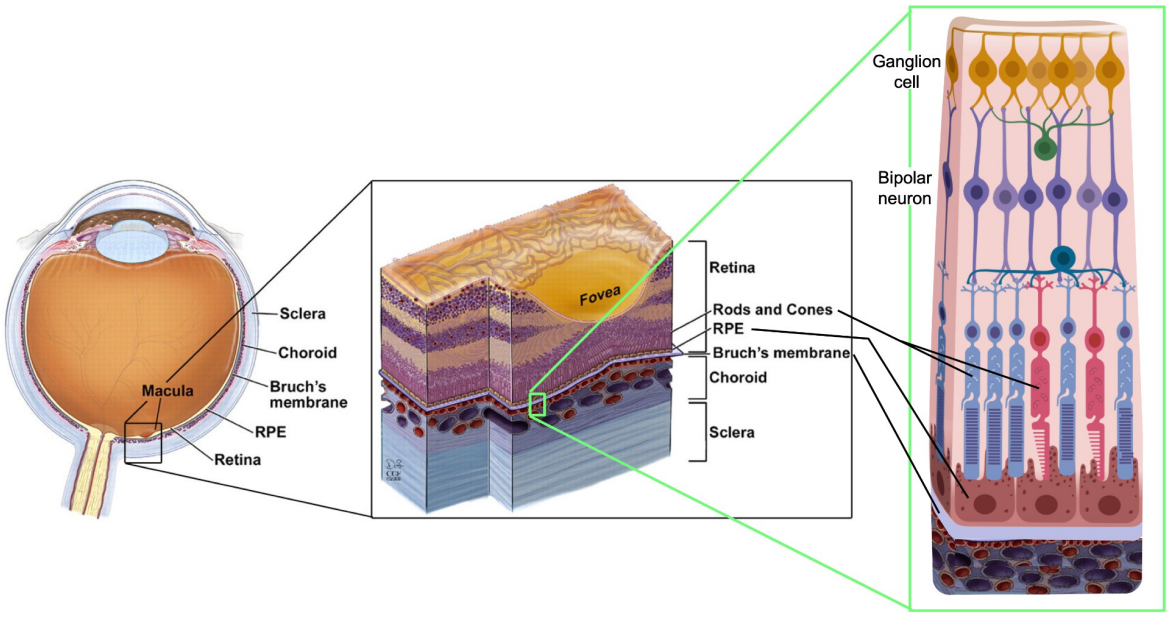

Figure 1.2 - Eye and retinal structure. Schematic of the human eye (left), macular cross-section (center), and cellular organization (right). The macula and fovea are highlighted, along with key layers including the sclera, choroid, Bruch's membrane, RPE, and photoreceptors. Retinal neurons (rods, cones, bipolar cells, and ganglion cells) transmit visual signals to the brain. Image created in part using Biorender.com.

This degeneration occurs because when the human body ages, the overall structural and functional integrity of the RPE and Bruch's membrane declines, making it increasingly difficult to maintain a healthy retina (Figure 1.3). As clearing waste becomes less efficient, a yellow lipid containing deposit called drusen begins to accumulate between the RPE and Bruch's membrane [7]. Simultaneously, the Bruch's membrane starts to thicken and stiffen due to collagen cross-linking and lipid accumulation, further hindering nutrient transport and waste clearance [7]. As AMD progresses, metabolic byproducts build up due to impaired waste clearance and contribute to drusen formation. One byproduct is amyloid beta, an important component of drusen, which is known to accumulate with age not only in the retina but in the central nervous system (CNS) as well [4,6]. Over time, increased amyloid beta deposits have been found in areas such as the Bruch's membrane, retinal vasculature, and outer segments of photoreceptor cells [17]. As a result, the Bruch's membrane starts to deteriorate as its elastin and collagen start to degrade and its matrix begins to calcify [7]. These changes to the Bruch's membrane can result in the physical and functional separation of photoreceptors and RPE cells from their blood supply, signaling the development of AMD and failure of the RPE.

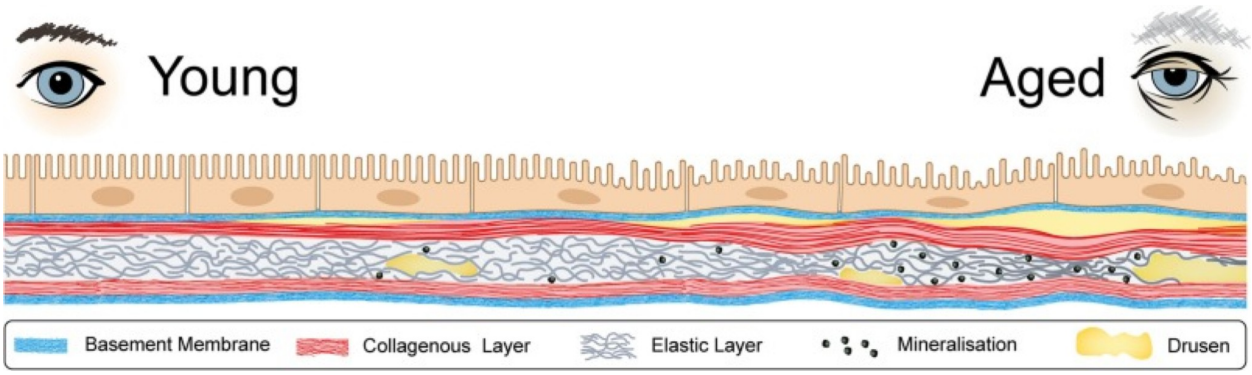

Figure 1.3 - Structural changes in Bruch's membrane and the retinal pigment epithelium (RPE) with aging. Blue – Basement membrane; Red – Collagenous layer; Gray – Elastic layer; Black dots – Mineralization; Yellow deposits – Drusen. [81]

AMD can be divided into 4 stages [13,24]. The first stage, described in the previous passage, starts with Bruch's membrane malfunctioning, resulting in drusen build up. These deposits in this stage are characterized as large and soft. In the second stage, drusen begins increasing in number, becoming smaller and harder. The third stage is marked by the emergence of abnormalities within the RPE, indicating increasing cellular dysfunction. Lastly, the fourth and final stage known as advanced AMD can be characterized by geographic atrophy in the fovea, leading to significant visual impairment. At this stage, the RPE and photoreceptors are degenerated, resulting in irreversible central vision loss. As AMD runs through the stages, RPE cells will either die off and atrophy or they will signal for help. This degeneration of the eye can be classified into two types: atrophic (dry) and neovascular (wet).

1.2. Existing Treatments for AMD

Wet AMD begins when RPE cells that are under stress start signaling for help by releasing substances such as vascular endothelial growth factor (VEGF), triggering new abnormal blood vessels to enter into the retina [2,13]. This process is known as choroidal neovascularization. Even though this is the RPE's attempt to restore its blood supply, these newly formed vessels are not structurally sound and are highly leaky, releasing large amounts of fluid in and around the structures of the retina that further distort vision (Figure 1.4). This surplus of fluid build-up is precisely why the condition is called "wet" AMD. This rapid accumulation of blood within the eye results in damage to the photoreceptor cells. The persistent

accumulation of fluid damages the photoreceptor cells by disrupting the exchange of nutrients and waste between the RPE and the choriocapillaris, depriving photoreceptors of the metabolic support they require to function. Over time, this sustained disruption accelerates photoreceptor degeneration, leading to progressive and irreversible loss of central vision.

In the worst cases these vessels burst, leading to macular hemorrhage [2]. Damage due to macular hemorrhage comes from iron mediated oxidative stress following hemoglobin breakdown, which is the disruption of the exchange between nutrients and waste, and clot contraction that mechanically compresses and disfigures retinal tissue [64,65]. Overall, these mechanisms create a toxic microenvironment that speeds up photoreceptor degeneration and puts the retina in grave risk. A macular hematoma can also form in the sub-RPE, found under the RPE layer. Large detachments of the RPE further worsen the condition by agitating the structure of the macula.

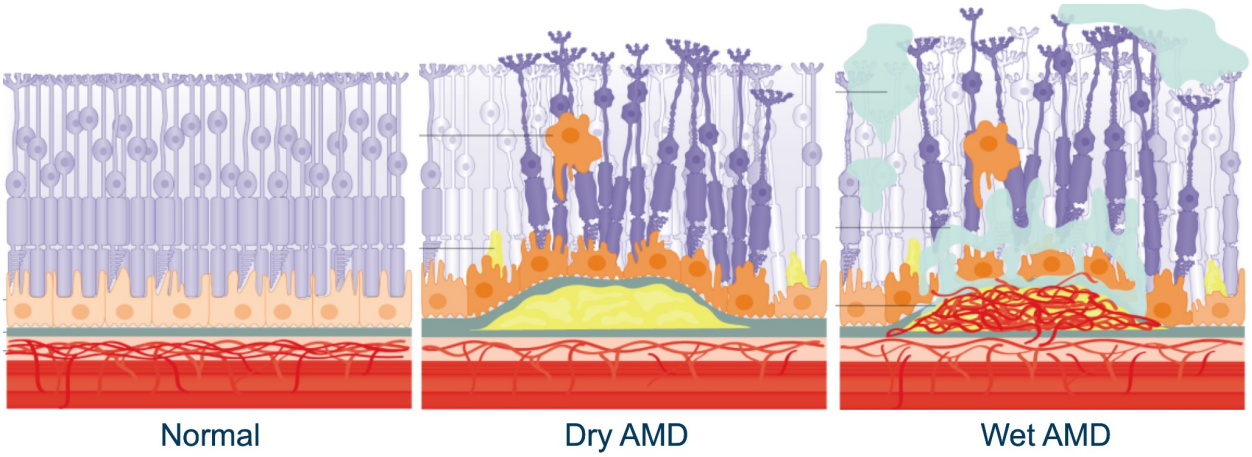

Figure 1.4 - Progression of age-related macular degeneration (AMD) from normal retina, to dry AMD and then wet AMD. Dry AMD is characterized by drusen accumulation and RPE disruption, while wet AMD involves choroidal neovascularization and leakage beneath the retina. Dry AMD does not always progress to wet AMD. [82]

The presence of drusen, edema, and hemorrhage are significant barriers that prevent light from reaching the photoreceptors, causing a decrease in visual acuity.

There have been various approaches to treat wet AMD such as photodynamic therapy and the use of

drugs. Photodynamic therapy targets newly formed abnormal blood vessels by activating a photosensitizing agent that is delivered intravenously and selectively absorbed by the rapidly growing endothelial cells of the choroidal neovascular membrane [34]. Once activated by a specific wavelength of light, the agent produces reactive oxygen species that damage and occlude the abnormal vessels, effectively canceling out choroidal neovascularization while maintaining the viability of both the RPE cells and the neural retina. This therapy avoids visual field defects and central visual impairment, which is a common symptom of AMD. Unfortunately, the downsides to this treatment include temporary visual impairment and photosensitivity reactions [34].

Other treatments for wet AMD involve anti-VEGF medications that block the VEGF protein. Typically, these drugs are administered via intravitreal injections (Figure 1.5) and are available as agents such as ranibizumab and aflibercept [8,27]. When VEGF activity is inhibited, there is reduced vascular leakage and the progression of neovascular damage is limited. Targeted anti-VEGF drugs are the first line of defense treatments for wet AMD, and it has been shown to reduce the rate of vision loss within patients [8,32]. With that being said, some patients do not respond to these treatments or continue to experience a decline in visual acuity despite ongoing therapy [66]. Although it is the only treatment with few side effects, the treatment is not perfect by any means.

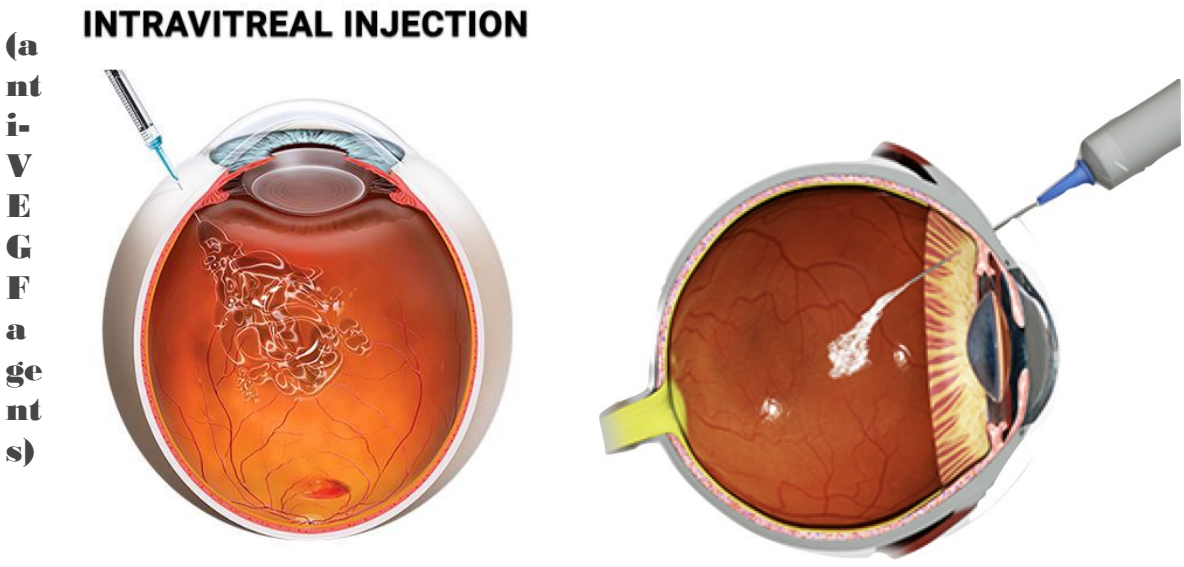

Figure 1.5 - Schematic illustration of intravitreal injection of anti-VEGF agents for the treatment of wet AMD. Left: Anatomical cross-section of the eye demonstrating the injection route through the pars plana into the vitreous cavity, targeting the site of choroidal neovascularization in the posterior segment. Right: Alternate view.. Intravitreal anti-VEGF therapy represents the current gold-standard treatment for wet AMD, acting to inhibit pathological angiogenesis and reduce vascular leakage, thereby preserving and potentially improving central vision. [82,83,84]

Anti-VEGF treatment requires frequent intravitreal injections, which can be burdensome for patients and may produce varying responses depending on the individual. The financial cost of repeated injections can also be significant, and the cumulative nature of the treatment carries risks of procedure-related complications such as endophthalmitis, retinal detachment, and intraocular pressure elevation, all of which become increasingly concerning with long-term repeated administration [30].

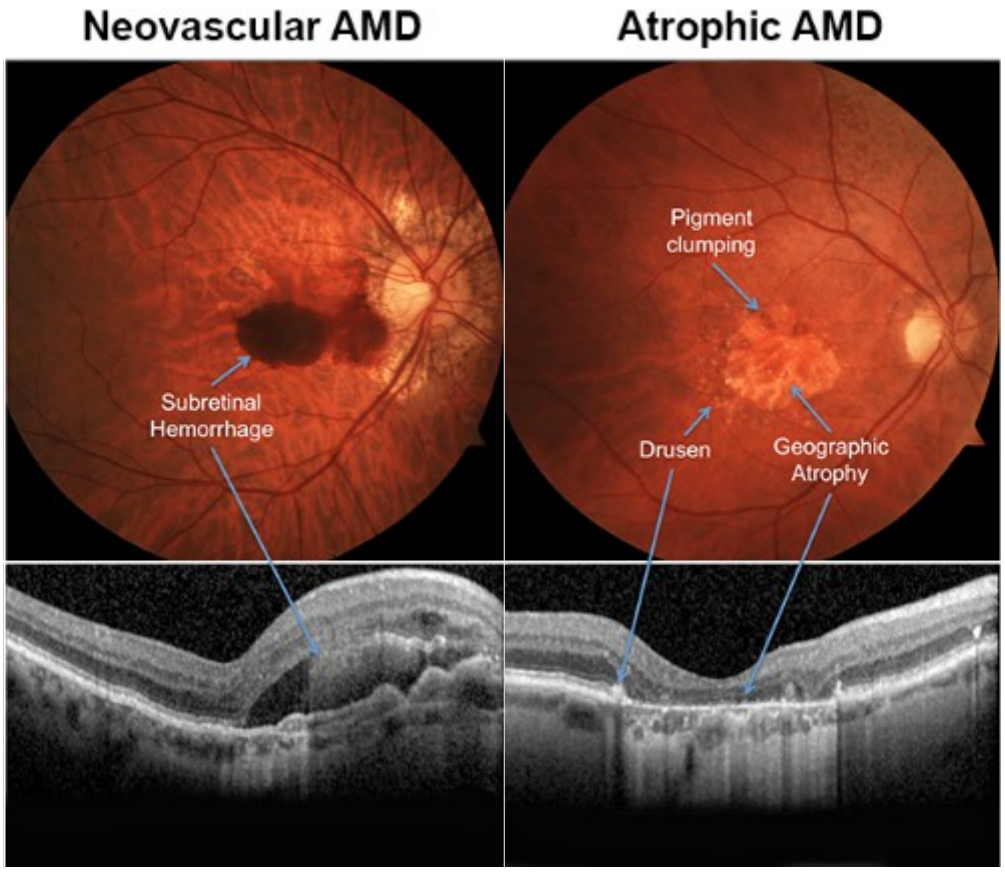

Figure 1.6 - Top images show fundus (inner back surface of the eye) photographs. Bottom images show corresponding Optical Coherence Tomography (OCT) scans, a non-invasive imaging technique that uses near-infrared light waves to capture high-resolution cross-sectional images of the retinal layers. Top Left: Fundus photograph showing wet (neovascular) age-related macular degeneration (AMD), characterized by submacular hemorrhage, hard exudates, and choroidal neovascularization in the macular region. Top Right: Fundus photograph showing dry (atrophic) AMD, characterized by multiple macular drusen deposits appearing as yellowish-white subretinal pigment epithelium accumulations, with preserved optic disc and retinal vasculature. Bottom Left: The OCT scan for neovascular AMD reveals subretinal fluid accumulation and disruption of the retinal layers characteristic of active choroidal neovascularization. Bottom Right: The OCT scan for atrophic AMD demonstrates thinning and loss of the outer retinal layers and retinal pigment epithelium, consistent with geographic atrophy. [85]

On the other hand, dry AMD occurs when RPE cells fail to call for help and this results in the loss of retinal structures as the RPE is separated from its blood supply. Debris from the drusen can enter the subretinal space, known as “drusen ooze,” which leads to an excess of debris between the RPE and the vasculature, leading to the death of RPE [67]. The death of these cells leads to geographic atrophy, resulting in permanent damage to central vision. Dry AMD can be characterized by sharply demarcated regions of macular dysfunction, with progressive degeneration of the RPE. These expand over time, resulting in irreversible central vision loss. Areas affected by geographic atrophy correspond to absolute scotomas, where visual perception is completely absent [68]. At this stage, central vision loss has already been irreversibly compromised, and continued expansion of these atrophic regions only deepens the extent of that damage.

In spite of significant advances in understanding the molecular mechanisms of dry AMD, there remains no cure that can restore lost retinal tissue. Current therapeutic efforts mainly focus on slowing disease progression, preserving residual vision, and overall managing associated risk factors rather than achieving regeneration. In 2023, the U.S. Food and Drug Administration approved the first pharmacologic treatments specifically for geographic atrophy: pegcetacoplan (Syfovre), a complement C3 inhibitor, and avacincaptad pegol (Izervay), a complement C5 inhibitor, both delivered by intravitreal injection and shown to reduce the rate of geographic atrophy lesion growth compared with sham treatment in clinical trials [35,36]. These agents work by targeting dysregulation of the complement system, which is a key driver of the chronic local inflammation and progressive tissue breakdown that characterizes AMD. However, they are unable to reverse retinal damage that has already occurred.

Both wet and dry AMD are preceded by the loss of function of the Bruch's membrane, a structure that

plays a fundamental role in sustaining RPE health and overall retinal homeostasis [7]. In a healthy eye, the Bruch's membrane acts as both a structural and functional scaffold, providing the mechanical stability needed for RPE cell polarization, attachment, and survival through its layered configuration of collagen and elastin fibers. As the Bruch's membrane deteriorates, the RPE becomes increasingly metabolically stressed, triggering a cascade of events that ultimately results in photoreceptor degeneration and the vision loss characteristic of both wet and dry AMD. Given that Bruch's membrane dysfunction lies at the heart of AMD progression, many regenerative strategies have shifted their focus toward restoring or replacing this critical interface. Scaffold-based approaches, in particular, are designed to recapitulate the structural and functional properties of the native Bruch's membrane, providing a supportive substrate upon which RPE cells can attach, polarize, and resume their normal physiological functions. By mimicking the architecture and permeability of the Bruch's membrane, these scaffolds aim to restore the homeostatic environment that the RPE requires to sustain photoreceptor health and shield against vision loss.

1.3. Scaffolds as Replacement Bruch's Membranes

Several studies have increasingly focused on scaffold-based strategies for RPE replacement as a therapeutic approach for AMD [26]. A 2023 study investigating microfabricated polyglycerol sebacate (PGS) scaffolds describes honeycomb-patterned biodegradable substrates designed to support the co-delivery of human pluripotent stem cell-derived RPE cells and photoreceptors to the subretinal space [19]. Unlike a permanent Bruch's membrane substitute, the PGS scaffold is intentionally biodegradable. Following implantation, it undergoes gradual hydrolytic and enzymatic breakdown into sebacic acid and glycerol, both of which are naturally occurring mammalian metabolites, with full degradation expected within 30 to 60 days in the subretinal space. As such, the scaffold serves as a temporary structural vehicle to organize and deliver the cells to the target site, after which it degrades and leaves behind the transplanted cell layers to integrate with the host tissue.

Majidnia et al. designed an electrospun polycaprolactone (PCL) collagen scaffold to mimic the Bruch's membrane and support overall RPE monolayer formation [21]. Their results demonstrated that the

scaffold improved RPE attachment, organization, and functional stability compared to non-scaffold conditions. In a 2023 study, Egbowon et al. demonstrated that electrospun nanofiber scaffolds composed of polyacrylonitrile treated with fluocinolone acetonide, an anti-inflammatory glucocorticoid agent, enhanced the growth, differentiation, and overall functionality of RPE cells, with cells retaining their characteristic morphology and remaining viable for up to 150 days [12]. The authors proposed this system as a potential Bruch's membrane substitute, offering a synthetic, non-toxic, and biostable support for RPE cell transplantation. However, the study acknowledged several important limitations. First, the work was conducted using the ARPE-19 immortalized cell line, which raises concerns regarding cellular heterogeneity, meaning that the results may not fully reflect the behavior of primary human RPE cells or hiPSC-derived RPE cells, which are considered more physiologically representative for transplantation purposes [69]. Second, the study did not assess cell polarity, which is considered critical for RPE cells to support the neural retina and maintain access to the choroidal blood supply [18]. Third, the system was not tested for biocompatibility with human tissue, and all findings remained limited to in vitro conditions. Finally, the authors noted that producing a suitably thin membrane of approximately 5 μm for implantation into the subretinal space remains a key fabrication challenge [12].

1.4. Tissue Engineering Approaches to AMD treatments

Scaffold-based efforts fit within the broader field of tissue engineering (Figure 1.7) [38,39], which seeks to replace or restore damaged tissues through the strategic integration of cells, biomaterials, and biochemical or mechanical cues. For AMD applications in particular, tissue engineering aims to recreate the structural and functional features of the native RPE and/or Bruch’s membrane interface, rather than simply supplying passive structural support. For example, Rickabaugh et al. engineered a biomimetic in vitro model of a Bruch's membrane using recombinant hagfish intermediate filament (rHIF) proteins [25]. The membranes were evaluated for their mechanical properties, permeability, and capacity to support RPE cell culture, and were demonstrated to accurately mimic both healthy and aged Bruch's membrane for in vitro modeling of the subretinal tissue.

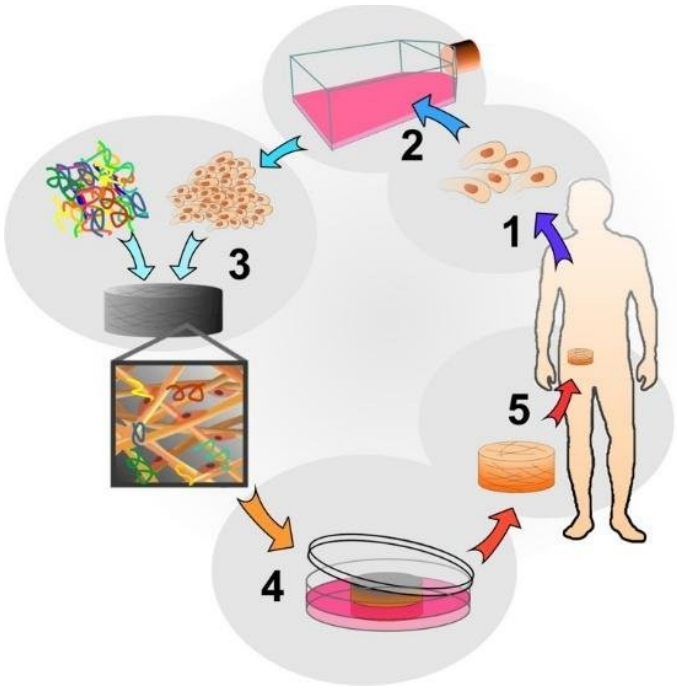

Figure 1.7 - Schematic overview of the tissue engineering paradigm. Tissue engineering for the retina might involve: (1) harvest of somatic cells from the patient via skin biopsy, (2) reprogramming and culture of cells in specialized bioreactors to generate induced pluripotent stem cells (iPSCs), (3) directed differentiation of iPSCs using growth factors and signaling molecules toward an RPE cell lineage, (4) seeding and maturation of the differentiated RPE cells onto a biocompatible scaffold or membrane, and (5) transplantation of the engineered RPE construct back into the patient's subretinal space. This autologous approach minimizes the risk of immune rejection and represents a promising therapeutic strategy for the restoration of RPE function in AMD. [86]

Correspondingly, Zimmermann et al. investigating electrospun polycaprolactone (PCL) and PCL-collagen nanofiber scaffolds analyzed their ability to support long-term RPE cell culture using porcine-derived cells [33]. The result from the study showed that the RPE cells cultured on these scaffolds maintained stable morphology, low inflammatory cytokine expression, and viability for up to one year, potentially hinting that such biomimetic substrates can sustain key physiological properties necessary for transplantation. However, the authors noted that maintaining full functional activity and controlling inflammatory responses remain ongoing challenges.

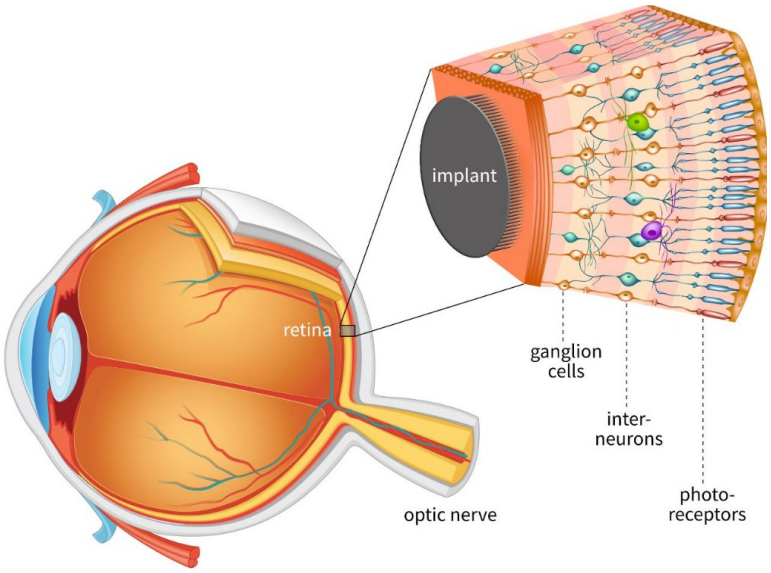

Figure 1.8 - Schematic illustration of a retinal implant positioned within the eye. *(Left)* Cross-sectional view of the human eye depicting the anatomical location of the retina and optic nerve. *(Right)* Magnified view of the retinal layers showing the placement of the implant in relation to the cellular architecture of the retina, including the ganglion cells, interneurons, and photoreceptors. The implant interfaces with the remaining retinal circuitry to electrically stimulate surviving cells, bypassing degenerated photoreceptors to restore partial visual signaling via the optic nerve to the brain. Such retinal prosthetic devices represent an emerging therapeutic approach for advanced retinal degenerative conditions, including end-stage age-related macular degeneration (AMD). [87]

In a more reproducible approach, a 2025 review by Li et al. combined current advancements in cell based and cell biomaterial scaffold approaches for AMD [37], emphasizing the development of these complex scaffolds that implement both RPE and photoreceptor precursors for potential subretinal implantation. The article added that cell biomaterial scaffolds have been widely used in order to promote reintegration of cells at the damaged site. It also addresses the cons of translocation and discrete cellular structure caused by cell injection, however, these therapeutic strategies have only shown initial success and have not yet been tested long term. Preclinical validations and clinical trials are a must to confirm their long term safety, functional durability and consistency.

While these advanced scaffold structures can support cell organization, survival, and some level of function, getting enough oxygen and nutrients to cells and overall long term function still remains a difficult challenge [70]. A simple minor disruption to these processes can greatly accelerate degeneration, showing why scaffolds need to be optimized in order to balance mechanical support with biological performance in the diseased retina. The choice of the biomaterial itself is central to this optimization, due

to it directly determining how well the scaffold reacts biologically as well as its capability for clinical translation.

1.5. Natural vs. Synthetic Scaffolds for Tissue Engineering

The choice of a biomaterial scaffold is an important factor to consider given that it influences biological performance and whether the material is suitable for clinical use. Typically these scaffolds can be split between either natural or synthetic. In general, natural biomaterials such as collagen, fibrin, and chitosan are inherently biocompatible and often contain sites that cells can recognize and attach to, making them well suited for cell mediated tissue regeneration and native microenvironments [43]. When considering replacements for the Bruch's membrane, researchers have explored several of these materials as potential scaffolds.

Silk fibroin in particular has been explored as a Bruch's membrane substitute, specifically by Shadforth et al., who cultured ARPE-19 RPE cells on fibroin membranes that were manufactured to a thickness of 3 μm, similar to that of native Bruch's membrane [28]. The results showed that the cells developed characteristic cobblestone morphology with partial pigmentation and overall maintained key physiological functions which consist of phagocytosis and VEGF secretion over four months in vitro.

Building on this, Shadforth et al. further explored the addition of human recombinant tropoelastin into silk fibroin membranes in order to better mimic the elastic-rich structure of native Bruch's membrane [41]. This shows that tropoelastin could be effectively combined into the fibroin matrix while supporting its structural integrity and suitability for RPE cell support. On top of that, Belgio et al. produced a Bruch's membrane model by electrospinning a mix of Bombyx mori silk fibroin and polycaprolactone [5]. This process produced membranes with high porosity and a fiber diameter of approximately 1217 nm onto which ARPE-19 cells successfully adhered and spread, proposing the construct as the basis for a three-dimensional in vitro retinal model for AMD research. Galloway et al. established functional hiPSC-RPE monolayers on Bombyx mori silk fibroin scaffolds coated with extracellular matrix proteins [42], demonstrating that cells from five distinct hiPSC lines maintained RPE-characteristic morphology, pigmentation, gene expression, and functional properties for over three months in longitudinal

experiments, supporting the potential of silk fibroin as a prosthetic Bruch's membrane for both in vitro disease modeling and in vivo cell replacement therapy.

Collagen and fibrin hydrogels have also been examined, specifically as natural scaffolds for outer retinal reconstruction. Dujardin et al. used a fibrin scaffold in order to support the co-culture of primary human retinal microvascular endothelial cells and choroidal fibroblasts [40]. A layer of hiPSC-derived RPE cells was then seeded on top of this vascular structure, rebuilding the layered cellular organization of the outer blood-retinal barrier. The resulting co-culture displayed well-defined intercellular tight junctions and enhanced expression of RPE-specific markers compared to monoculture conditions. Additionally, Gandhi et al. showed that high concentration human fibrin hydrogels are safe and degradable scaffolds that are capable of supporting RPE monolayer growth in vitro [14]. The group further displayed that when cell-free fibrin hydrogels were implanted into the subretinal space, they degraded naturally without triggering an inflammatory response [15]. These findings established fibrin as a promising degradable alternative to the non degradable synthetic scaffolds that are currently being used in RPE transplantation. Separately, Wei et al. investigated four biodegradable hydrogels, specifically gelatin methacrylate (GelMA), hyaluronic acid methacrylate, sodium alginate, and fibrin, as potential carriers for human embryonic stem cell-derived RPE cells [31]. Of the four materials tested, fibrin was identified as the most suitable scaffold. It supported RPE cell adhesion, proliferation, and barrier function formation, while also promoting the expression of proteins critical for retinal function, making it the strongest candidate among the group for RPE transplantation applications.

Due to the fact that natural biomaterials are derived from the extracellular matrix of plant or animal tissues, they closely resemble the human body's own extracellular matrix and contain intrinsic biochemical and microarchitectural cues. Therefore, they can enhance overall cellular responses and integration. However, because these materials are highly processed for sterility and handling purposes, they typically suffer from inconsistent properties between batches, limited mechanical strength, and overall difficulty controlling how fast they degrade [43]. In addition, with natural materials there are numerous biological factors and cues, making it impossible to tease out exactly what is required for a healthy and functional RPE. As a result, attaining reproducible results when using natural materials can

be challenging.

On the other hand, synthetic biomaterials such as polylactic acid (PLA), polyglycolic acid (PGA), polylactic-co-glycolic acid (PLGA), and polyethylene glycol (PEG), can be precisely engineered. These materials' chemical compositions, mechanical properties, structure and degradation rates can be accurately controlled, enabling tailored design for specific applications. As a result, synthetic scaffolds are easily reproducible and tunable, however, they lack intrinsic natural biological signals that promote cell attachment and function [43]. Overall, even though both natural biomaterials such as collagen, fibrin, silk fibroin, and chitosan, and synthetic biomaterials such as PLA, PGA, PLGA, and PEG, each offer distinct advantages, neither alone fully meets the structural, biological, and mechanical demands required for retinal tissue engineering. This limitation has led to increased interest in hybrid and composite materials that combine biological activity with structural tunability [71].

1.6. Polyethylene Glycol Hydrogels as Scaffolds

In tissue engineering, PEG-based hydrogels are often considered to be a biologically inert "blank slate", and this is due to their resistance to protein adsorption, which cells require to recognize and bind to. Due to the fact that proteins cannot readily adsorb onto PEG surfaces, cell adhesion is not possible. As a result, PEG hydrogels do not trigger an immune response or inflammation [72]. This blank slate feature of PEG gives researchers the ability to modify individual features of their hydrogels, permitting the direct matching of hydrogel characteristics with cell response. This allows researchers the ability to build fully customized and reproducible scaffolds from scratch. An important advantage of PEG as a blank slate material is its high tunability. Its physical and chemical properties, including stiffness, degradation rate, and mesh size, can be independently controlled and precisely engineered to match the mechanical and structural needs of the targeted native tissue [72]. Additionally, PEG hydrogels are highly hydrophilic, forming highly hydrated structures that are physically reminiscent of the native extracellular matrix [72]. Overall, PEG hydrogels serve as a versatile and modular platform for dissecting how individual scaffold features influence cell behavior and for designing biomaterials with defined biological activity.

Because PEG is intrinsically inert, it requires modification to be biologically active. For instance, PEG can

be functionalized with the fibronectin-derived Arginine-Glycine-Aspartic acid-Serine (RGDS) adhesion peptides to permit cellular attachment [16]. When researchers functionalized PEG and modified only its stiffness, subsequent cellular responses could be attributed solely to the difference in stiffness [11]. Additionally, PEG hydrogels have been modified with matrix metalloproteinase (MMP)-sensitive peptide linkers, giving cells the ability to locally degrade and remodel the scaffold, which has been shown to affect cell migration and tissue formation [20]. Growth factors have also been incorporated into PEG hydrogels to modulate cellular activities such as proliferation, differentiation, and tissue-specific gene expression, further expanding the biological functionality of the scaffold [44]. Researchers tune the stiffness of PEG hydrogels to study mechanotransduction; by altering crosslinking density while keeping biochemical signals constant, changes in cell behavior can be directly attributed to mechanical properties such as stiffness [11].

1.7. Scaffold Mechanical Properties

Crosslinked PEG hydrogels are typically elastic in nature, which means they will always return to their original shape/state after deformation, and this occurs without the hydrogel dissipating energy nor exhibiting any time dependence to its physical properties [53]. This behavior does not fully represent the complex nature of biological tissues however. In vivo, the extracellular matrix demonstrates viscoelastic behavior which, unlike elasticity, is a time dependent mechanical behavior that allows for stress relaxation and energy to dissipate [53]. Viscoelasticity allows tissues to respond to mechanical forces in a dynamic way across a multitude of timescales and this behavior more accurately reflects the physiological conditions that cells experience in their natural environment [53].

Multiple studies have shown that cell behavior can be regulated by both substrate stiffness and viscoelastic properties such as stress relaxation [45,46,48]. Hydrogels that demonstrate stress relaxation have been shown to regulate important cellular processes which include spreading, proliferation, migration and differentiation, even when elastic modulus is held constant [45,47]. Most notably, viscoelastic networks that quickly relax can enhance cell spreading and cytoskeletal organization, implying that the rate of stress relaxation is an independent mechanical function that influences how cells react and respond to their surroundings.

Epithelial cells in particular are highly sensitive to viscoelastic cues. Studies have shown that epithelial cells that have been cultured on viscoelastic hydrogels have demonstrated altered migration behavior and enhanced mechanoactivation compared to epithelial cells that were on purely elastic hydrogels [49]. Furthermore, there is evidence indicating that epithelial cells themselves have displayed viscoelastic behavior, with their mechanical behavior depending on loading rate and time dependent deformation, and matching these properties is important for maintaining normal cellular function [50].

Age-related changes to the Bruch's membrane alter both its stiffness and its time-dependent mechanical properties, which can further impair RPE cell function [25,51]. However, many in vitro models still rely on elastic substrates, limiting their physiological relevance [51]. Given that RPE cells are a type of epithelial cell and share key features with other types of epithelial cells, including strong dependence on substrate interactions and mechanosensitivity, it is possible that RPE cells will respond more favorably to viscoelastic PEG hydrogels than to purely elastic systems. Specifically, viscoelastic substrates may enhance RPE cell spreading, viability, and function by more closely replicating the native retinal microenvironment. PEG hydrogels can be engineered to exhibit viscoelastic behavior through dynamic or reversible crosslinking, enabling independent control over stiffness and stress relaxation [73]. Using PEG preserves the advantages of synthetic tunability while introducing biologically relevant mechanical cues [53,72]. Therefore, this work develops a viscoelastic PEG-based hydrogel towards achieving a viscoelastic PEG-based scaffold for RPE cells.

CHAPTER 2. Literature Review

Hydrogels are three-dimensional crosslinked polymer networks that are capable of absorbing and retaining large amounts of water without dissolving, creating a highly hydrated structural framework that closely mimics the physical and chemical environment of native biological tissues [52]. Elastic hydrogels are elastic due to their stable covalently crosslinked structure. Viscoelastic hydrogels obtain viscoelasticity through network rearrangements or polymer disentanglements and sliding. Such viscoelasticity is most pronounced in hydrogels with non-covalent or dynamic covalent interactions. Conventionally crosslinked hydrogels can only achieve limited amounts of viscoelastic behavior due to their high water content and restricted polymer movement, making it necessary to engineer hydrogels that better replicate the

viscoelasticity of native ECMs [53].

One method to form viscoelastic hydrogels is to incorporate into the polymer network interactions that allow the biomaterial to rearrange over a period of time, such as reversible ionic bonds and supramolecular associations. These interactions allow for stress relaxation and deformation over time. Chaudhuri et al. engineered ionically crosslinked alginate hydrogels [45]. Ionic crosslinking is a form of physical crosslinking (or reversible crosslinking) because the bonds rely on electrostatic attractions rather than permanent atomic sharing as with covalent crosslinking. The study showed that the stress relaxation half-time ($\tau_{1/2}$) was modified from approximately one hour to one minute by changing the molecular weight of the alginate polymer and incorporating PEG spacers, while holding the initial elastic modulus constant. By using this method, mesenchymal stem cells (MSCs) encapsulated in fast relaxing alginate hydrogels were shown to undergo predominantly osteogenic differentiation, while MSCs in slow relaxing hydrogels underwent a predominantly adipogenic differentiation instead, with minimal osteogenic markers present. This contrast shows that stress relaxation, which is independent of stiffness, is a key regulator of stem cell fate in 3D culture [54].

Lou et al. created a hydrogel that possesses an interpenetrating network and consists of hyaluronic acid crosslinked with dynamic covalent bonds combined with collagen I. They found that hydrogels with faster stress relaxation caused more cell spreading, more fiber remodeling and more focal adhesion formation than hydrogels that had slower stress relaxation rates [54]. Similar to elastic hydrogels, viscoelastic hydrogels can be divided into natural and synthetic polymer based networks. Natural biomaterials such as hyaluronic acid, chitosan, alginate, and collagen are inherently slightly viscoelastic due to their polymer networks relying on reversible physical interactions which include hydrogen bonding, ionic interactions, and/or chain entanglement [53]. Hyaluronic acid hydrogels specifically have been widely researched as viscoelastic systems for stem cell culturing, with articles showing that viscoelastic hyaluronic acid hydrogels promoted more regional patterning of human pluripotent stem cell derived organoids compared to elastic hydrogels. It was also found that faster stress relaxation increases nuclear localization of Yes-associated protein (YAP), which is a mechanosensitive transcription factor [55, 57].

Nam et al. showed that stress relaxation within hydrogels made of alginate could be precisely altered by

covalently inserting PEG chains onto the alginate backbone. By increasing the PEG concentration as well as the molecular weight, the hydrogel had a faster stress relaxation rate and also a higher loss modulus, offering a simple and controllable method to adjust viscoelastic properties in 3D cell culture systems [56]. Natural hydrogels, however, still face several limitations despite these advantages. They tend to have low mechanical strength, inconsistencies from batch to batch, and are difficult to control in terms of degradation rate and stiffness, causing these hydrogels to have complications in reproducibility, which adversely impacts large scale manufacturing [43].

Synthetic polymers like polyacrylamide (PA), polyvinyl alcohol (PVA), and PEG can be precisely tuned to control certain aspects of the polymer, which include control network architecture, crosslink density, and mechanical behavior [74]. Viscoelasticity is typically implemented into these synthetic polymers by using dynamic crosslinking processes. For example, Tang et al. demonstrated that boronate ester-based adaptable hydrogels exhibit fast relaxation with time constants on the order of seconds, while remaining stable for long-term cell culture [57]. The authors also showed that these fast-relaxing matrix mechanics promoted cell spreading, increased nuclear volume, and YAP nuclear localization in human MSCs, driven entirely by the cells' ability to physically remodel their surrounding microenvironment. Similarly, Sinha et al. developed a PEG-based hydrogel system crosslinked with hydrazone bonds of tunable kinetics, in which the ratio of alkyl-hydrazone to benzyl-hydrazone bonds was used to control the rate of stress relaxation They demonstrated that increasing stress relaxation in 3D promoted invasive behavior of glioblastoma cells including spreading and migration [60].

Conventional elastic PEG hydrogels are formed through permanent covalent crosslinking [53,72]. Several strategies have been described that introduce viscoelastic behavior into PEG hydrogels. McKinnon et al. utilized reversible hydrazone crosslinks as a strategy to introduce viscoelasticity into PEG hydrogels. In particular, they synthesized a PEG hydrogel in which the polymer chains were connected through bis-aliphatic hydrazone bonds, which is a type of reversible chemical bond that can break and reform over time, allowing the network to rearrange and dissipate stress. The resulting hydrogel was stress-relaxed, cytocompatible, and viscoelastic, and the hydrogel was then used to observe cellular forces and neurite outgrowth in encapsulated motor neurons [58, 59]. However, McKinnon et al. noted that because stress

relaxation in their system depended entirely on how fast the hydrazone bonds broke and reformed, it was difficult to tune the rate of stress relaxation independently from the stiffness of the gel, as changing one property inevitably affected the other.

Tang et al. implemented boronate ester crosslinks as another strategy to introduce viscoelasticity into PEG hydrogels. Boronate ester bonds are dynamic covalent bonds that can reversibly form and break under physiological conditions, enabling the network to rearrange and dissipate stress over time. Using fluoro-phenylboronic acid and nitrodopamine crosslinking, this research developed a fast relaxing PEG-based hydrogel that has a storage modulus of approximately 10 kPa and a relaxation time of approximately two seconds. In order to ensure the hydrogel remained stable during long term cell culturing, the network was further co-crosslinked through a secondary reaction which is known as strain-promoted azide-alkyne cycloaddition [57]. Despite that, a key limitation of this approach is its hypersensitivity to pH. Considering the ability of boronate ester bonds to form and break depends heavily on the surrounding pH, maintaining consistent mechanical properties at physiological pH of 7.4 is difficult, which complicates their use in biological applications [75].

The Caliari group's approach is by introducing viscoelasticity through supramolecular host-guest interactions. This type of interaction works similarly to a lock and key system, where one molecule, the host, has an opening that another molecule, the guest, fits into. In this method, an elastic hyaluronic acid hydrogel was first formed using a light-activated chemical reaction. Viscoelasticity was then introduced by adding adamantane-conjugated peptides into the hydrogel, which acted as guest molecules that inserted themselves into cyclodextrin host cavities already present within the network. Considering these host-guest bonds can constantly associate and dissociate, the network is able to rearrange and dissipate stress over time, establishing viscoelastic behavior while stiffening the hydrogel at the same time. This approach allowed the stiffness and viscoelastic properties of the hydrogel to be altered independently of one another [61]. However, a key limitation is that the rate of stress relaxation in host-guest systems can be difficult to control precisely, and the mechanical properties of the hydrogel may change over time as the balance between associated and dissociated host-guest bonds shifts under cell culture conditions [61].

Grad et al. took a network topology engineering approach as a fourth strategy. Rather than relying on the kinetics of bond exchange, they demonstrated that the architecture of the network itself could govern stress relaxation behavior. Specifically, a 4-arm star-PEG network crosslinked with coiled-coil peptides relaxed stress approximately two orders of magnitude faster than a polyisocyanopeptide fiber network using the same crosslink, because each elastically active chain in the star-PEG network contained only one crosslink, allowing full chain relaxation upon crosslink dissociation [62]. However, the synthesis of precisely defined star-PEG architectures requires complex multi-step functionalization procedures, which reduces the reproducibility and scalability of this approach [62].

Wang et al. introduced a fifth strategy by incorporating physical chain entanglement into a dual-network hydrogel, in which entanglement of high molecular weight PEG chains was combined with a permanent covalently crosslinked network. They demonstrated that the movement of entangled molecular chains between relaxed and tensioned states contributed to energy dissipation and viscoelastic behavior within this dual-network system [63]. However, controlling the degree of entanglement and achieving reproducible mechanical properties across batches remains an ongoing challenge, as entanglement density is highly sensitive to polymer concentration, molecular weight, and processing conditions [76].

Although these advances have been achieved, the majority of these viscoelastic PEG systems still rely on a permanent covalently crosslinked backbone, dynamic covalent chemistries, or complicated supramolecular formation to establish and stabilize the network, with physical entanglement serving only as a secondary or supporting contributor to viscoelasticity rather than the dominant mechanism [73]. For that reason, there is a need for a simpler and more controllable method in which physical entanglement itself drives stress relaxation, allowing the polymer network to rearrange over time without depending on a permanent covalent scaffold. To date, physical entanglement serving as the dominant source of stress relaxation in a PEG-based hydrogel system, independent of a permanent covalently crosslinked network, has not been reported in the literature as a standalone strategy for tissue engineering applications. This thesis describes the development of a viscoelastic PEG hydrogel in which stress relaxation arises primarily from physical entanglement within the polymer network, providing a new and simplified approach for designing PEG-based scaffolds with physiologically relevant mechanical properties.

CHAPTER 3. Materials and Methods

3.1. Experimental Design

This study's goal is to develop and classify a PEG-based viscoelastic hydrogel. In order to accomplish this, hydrogels were synthesized using polyethylene glycol dialdehyde (PEG - propionaldehyde) and polyethylene glycol diamine (PEG -amine), which form dynamic imine linkages once mixed together. The system was designed to promote physical entanglement of polymer chains during gelation, enabling stress relaxation behavior without the need for complex chemistries. In order to compare the viscoelastic properties of these viscoelastic hydrogels, a purely elastic PEG hydrogel was also formed, using polyethylene glycol diacrylate (PEGDA).

PEG precursor solutions were prepared at controlled concentrations and physiological pH conditions to facilitate imine bond formation. Hydrogels were formed by combining the two polymer solutions at a defined molar ratio and allowing gelation to occur under low-temperature conditions over an extended period. This approach was intended to encourage both network formation and polymer chain rearrangement, resulting in a viscoelastic material. Following synthesis, the mechanical behavior of the hydrogels was evaluated using qualitative and quantitative methods, including inversion testing and rheological analysis, to assess hydrogel formation and viscoelastic properties.

3.2. Materials

Unless otherwise noted, all polymers used were obtained from Laysan Bio, Inc (Arab, AL, USA) while reagents were obtained from Sigma Aldrich. Solution pH was adjusted using either sodium hydroxide or hydrochloric acid

3.3. Preparation of Prepolymer Solutions

Polyethylene glycol propionaldehyde (PEG-propionaldehyde, PALD-PEG-PALD, 5 kDa) and polyethylene glycol diamine (PEG-amine, NH_2-PEG-NH_2, 5 kDa) were used as the primary polymer components for hydrogel formation. Then phosphate-buffered saline with a pH of 7.4 (PBS; Gibco, ThermoFisher Scientific) was used as the solvent system for polymer dissolution. Sodium hydroxide (NaOH; Sigma Life Science) and hydrochloric acid (HCl; Sigma Life Science) were used to adjust the pH of the solutions when necessary. As for the elastic hydrogels, polyethylene glycol diacrylate (PEGDA, ACRL - PEG -

ACRL, 10 kDa) was used as the base polymer. Eosin Y disodium salt (1.0 mM) mixed with millipore water as well as 300 mg 2,2-dimethoxy-2-phenylacetophenone (acetophenone) dissolved in 1 mL 1-vinyl-2-pyrrolidinone (NVP) were used as a photoinitiator system in order to trigger crosslinking. Furthermore, a HEPES Buffered Saline (HBS) solution at a concentration of 25 mM was used as the solvent for the PEGDA solution. All reagents were used as received unless otherwise specified.

$$OCHCH_2CH_2O(CH_2CH_2O)_nCH_2CH_2CHO$$

Figure 3.1 - The chemical formula for Propionaldehyde-Poly(ethylene glycol)-Propionaldehyde.

$$NH_2(CH_2CH_2O)_nCH_2CH_2NH_2$$

Figure 3.2 - The chemical formula for Amine-Poly(ethylene glycol)-Amine.

3.3.1 Viscoelastic Hydrogel Solutions

Both the PEG-propionaldehyde and PEG-amine were stored at -20ºC and brought to room temperature prior to use. Separate prepolymer solutions of each polymer were prepared by dissolving either PEG-Propionaldehyde or PEG-amine in centrifuge tubes with 5 mL of PBS at 5%, 7%, and 10% (w/v) (Table 3.1).

Table 3.1: Prepolymer solution preparation. All solutions were prepared using 5 mL PBS.

Prepolymer solution	5% (w/v)	7% (w/v)	10% (w/v)
PEG-Propionaldehyde	0.25 g	0.35 g	0.5 g
PEG-amine	0.25 g	0.35 g	0.5 g

The pH of the solutions were then adjusted to approximately 6.8 to 7.2, which is a range that promotes dynamic imine bond formation between the aldehyde and amine functional groups. During the

experiments, it was observed that only the PEG amine solution required pH adjustment due to the solution being very basic. Small amounts of hydrochloric acid were then added to lower the pH to the desired range.

3.3.1 PEGDA Hydrogel Solutions

The acetophenone/NVP solution was prepared by dissolving 300 mg of acetophenone into 1 mL of NVP. This solution was then vortexed until fully dissolved and was stored in a foil-covered amber class vial at 4°C. A 1.0 mM eosin Y solution was prepared by dissolving approximately 6.92 mg of eosin Y disodium salt in 10 mL of millipore water, which was then stored in an amber 15 mL tube. To prepare the HBS solution, 1 mL of 1 M HEPES was diluted into 39 mL of millipore water to reach a final concentration of 25 mM. The final 10 % (w/v) PEGDA prepolymer solution was prepared by combining 0.1 g of PEGDA, 10 µL of acetophenone/NVP stock solution, and 1 mL of HBS solution in an amber 15 mL centrifuge tube, then vortexing the solution thoroughly after each addition to ensure uniform mixing.

3.4. Hydrogel Formation

Elastic and viscoelastic PEG hydrogels were formed and the rheological properties were assessed for each.

3.4.1 Viscoelastic Hydrogel Formation

The viscoelastic hydrogels were formed by mixing the PEG-propionaldehyde and PEG-amine solutions at a 1:1 molar ratio of reactive functional groups. Briefly, 0.5 mL of each solution was combined in an Eppendorf tube and gently vortexed. To increase polymer content and promote network formation, an additional 200 mg of each polymer was added to the combined solution, resulting in a final effective concentration of 50% w/v. The solution was again mixed by gentle vortexing to ensure uniform distribution of the polymer chains. Then the tube was sealed with parafilm and held at -20°C for 48 hours to gel.

3.4.2 Elastic Hydrogel Formation

A mold for the PEGDA hydrogels was created by placing a silicone spacer with a square cut-out in

between two microscope slides and tightly clamping the mold with alligator clips. The PEGDA solution was then drawn up using a 30 gauge needle and injected into the mold until completely filled. The filled mold was then placed under a UV light lamp and exposed for 2 minutes on each side to initiate photo-crosslinking via the Eosin Y and acetophenone/NVP photoinitiator system. Following light exposure, the clamps were removed and the glass slides were carefully separated. The formed PEGDA hydrogel sheets were removed using forceps, transferred immediately into PBS, covered in foil and stored at 4ºC until use.

3.5. Rheological Analysis

The viscoelastic properties of the PEG hydrogels were tested using both qualitative (inversion) and quantitative (rheology) methods. The hydrogel was taken out of the freezer and allowed to reach room temperature. Then the hydrogel tubes were inverted to assess hydrogel behavior under gravitational force. PEGDA hydrogel sheets were not subjected to inversion testing due to their sheet geometry and purely elastic nature.

Quantitative rheological measurements were conducted using a Discovery HR-2 hybrid rotational rheometer equipped with a 20 mm serrated steel parallel plate geometry. The 1.3 mL hydrogel samples were carefully loaded onto the plate stage and the upper plate with the geometry was slowly lowered until visual contact was reached. In order to ensure proper contact, the upper plate was further lowered until the axial force value was between 0.08-0.10 N, at which point plate movement was stopped to avoid unnecessary compression of the hydrogel. The final gap between the parallel plates was maintained at approximately 825-975 μm for all hydrogel samples and all measurements were performed at 25°C.

Oscillatory shear testing was then performed to analyze the viscoelastic behavior of the hydrogels. To start, oscillatory amplitude sweep tests were performed on each of the hydrogels, where all tests were conducted at a set frequency of 1.0 Hz, with the applied strain ranging from 0.01% to 100%. The purpose of this test was to properly identify the linear viscoelastic region (LVR), which is the strain range over which the storage modulus (G′) remained constant and steady. Based on this test, a fixed strain of 1% was selected for all following frequency sweep experiments thereafter, due to the fact that it fell within the LVR and would therefore not disturb the structure of the hydrogel during testing.

Frequency sweep experiments were then performed over a range of 0.1 to 100 Hz at a fixed strain of 1%. Storage modulus (G′) and loss modulus (G″) were recorded as a function of frequency to assess the elastic and viscous contributions of each hydrogel network. Both the PEGDA hydrogel and the PEG-propionaldehyde/PEG-amine hydrogel were tested under identical conditions to allow direct mechanical comparison between the two systems. All rheological measurements were performed on at least three independent samples to ensure reproducibility.

3.6. Hydrogel Degradation

PEG hydrogel degradation was analyzed gravimetrically in phosphate-buffered saline (PBS, pH 7.4). A total of 6 hydrogels of varying ages and storage conditions were evaluated for their degradation properties in separate wells. One hydrogel (Gel 1) was subjected to degradation tests 3 months following its formation. Two additional hydrogels (Gel 2 and Gel 3) were formed and stored at room temperature until testing 15 days later. Lastly, three hydrogels (Gel 4, Gel 5, and Gel 6) were tested 6 days after they were made. Gel 4 and Gel 5 were stored at −20°C until testing, while Gel 6 was stored at −20°C before being transferred to room temperature for 4 days prior to testing.

Each individual hydrogel was placed in separate transwells and weighed to obtain initial polymerized weight. Hydrogels were then partially submerged in PBS at 21°C and removed at successive time points for weight measurement. Measurements were obtained by briefly blotting excess PBS using a Kimwipe before weighing. Weights were recorded at approximately 10, 30, 60, and 70 minutes, then at 10-minute intervals until complete dissolution was observed. Hydrogel weight was normalized to initial weight and expressed as a percentage to account for variability in starting hydrogel size. Hydrogels were considered fully degraded when no intact material remained.

CHAPTER 4. Results

4.1 Hydrogel Synthesis and Qualitative Characterization

The viscoelastic hydrogels that were composed of 5K PEG-propionaldehyde and 5K PEG-amine were successfully synthesized. Following mixing, the solution remained in a liquid state at room temperature

and did not begin to gelate until it was placed at -20ºC, where the gelation process happened over 2-3 days, resulting in the formation of these viscoelastic hydrogels. This shows that successful formation of hydrogels was temperature dependent. Furthermore, hydrogels that remained at -20ºC for an additional 1-2 days were qualitatively observed to be firmer compared to the hydrogels that were removed earlier. Overall, the slow gelation process is consistent with the intended mechanism of physical chain entanglement occurring alongside dynamic imine bond formation between aldehyde and amine functional groups. Once the hydrogels were formed, they were translucent and had a pink/orange hue to them, as well as a visible increase in structural integrity, giving a clear indication of successful crosslink formation (Figure 4.1).

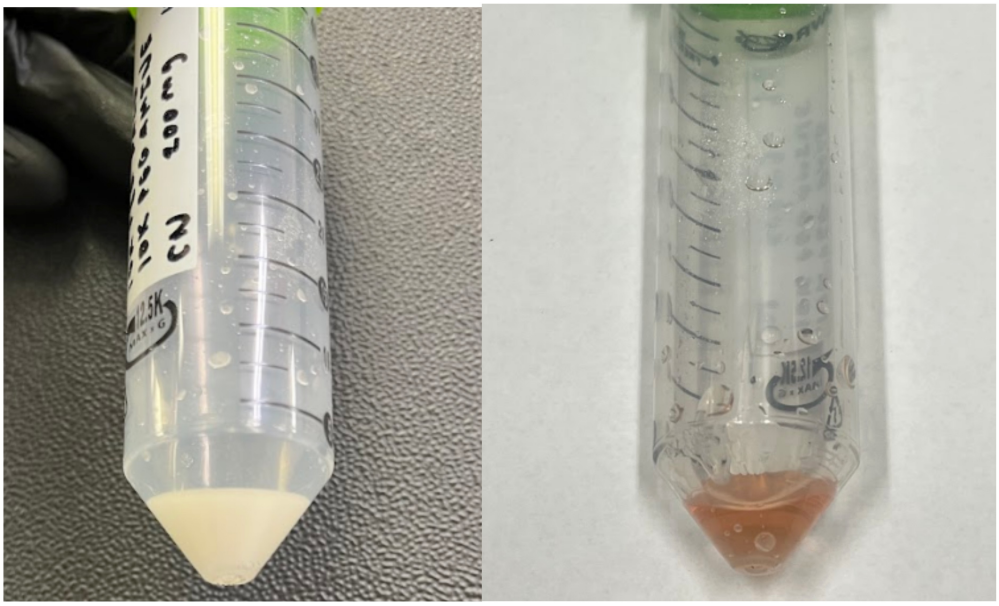

Figure 4.1 - PEG-based hydrogel before and after gelation. Left: Freshly prepared precursor solution immediately following mixing, appearing as an opaque white-cream liquid with apparent low viscosity. Right: The same formulation following gelation, displaying a translucent pale orange-tinted hydrogel with increased opacity and structural integrity, confirming successful crosslink formation and transition from a liquid to a viscoelastic solid state. The observable color and phase transition between the two samples was a visual indicator of successful hydrogel network formation, with the gelated sample demonstrating the characteristic physical properties required for further rheological and mechanical characterization.

When analyzing the qualitative tests, initially the hydrogels held their shape when the tube was inverted, however within 5 minutes, the hydrogel displayed a slow downward flow along the centrifuge tube's walls (Figure 4.2). This is indicative of a viscoelastic material, meaning that the material behaves as a solid over a short period of time, but acts viscously over longer periods of time. In addition, once the hydrogel

was removed from the tube and transferred onto a petri dish, the hydrogel initially held its shape before gradually spreading and flattening into a disc-like layer over time (Figure 4.3), further confirming its viscoelastic nature.

Figure 4.2 - Photographic demonstration of the inversion test used to test hydrogel formation and viscoelastic properties of PEG-based hydrogels. Hydrogels were fabricated by crosslinking polyethylene glycol propionaldehyde (PALD-PEG-PALD, 5 kDa) with polyethylene glycol diamine (NH_2-PEG-NH_2, 5 kDa) in phosphate-buffered saline (PBS). Left*:* The tube immediately following inversion, demonstrating initial solid-like behavior with the hydrogel remaining positioned at the top of the tube. Right*:* The same inverted tube showing flow after 2 min.

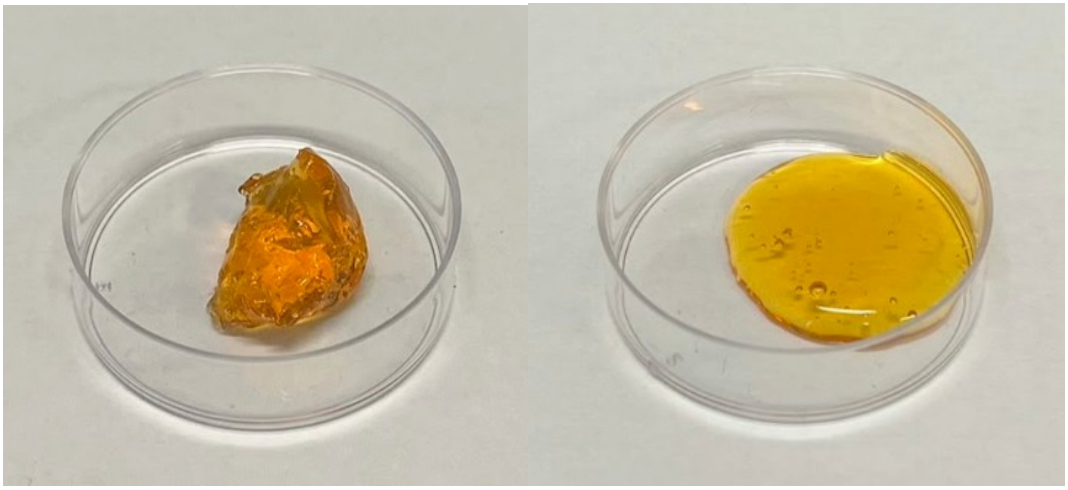

Figure 4.3 - The viscoelastic flow behavior of the PEG-based hydrogel over time. Left: The freshly shaped hydrogel retaining a defined three-dimensional form immediately after transfer from the tube to the dish. Right: The same hydrogel after 1 hour, demonstrating significant fluid-like flow and flattening into a thin, uniform disc-like layer under gravitational force.

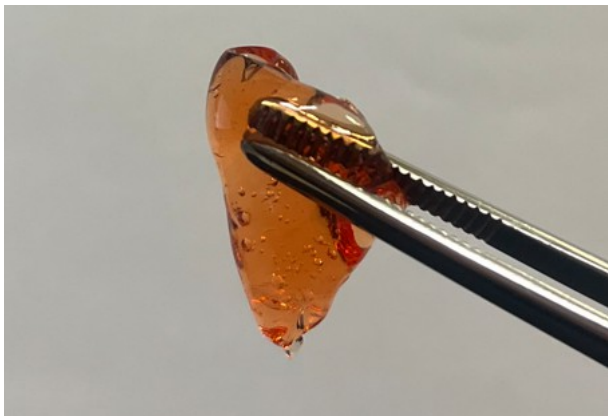

Figure 4.4 - A PEG-propionaldehyde/PEG-amine viscoelastic hydrogel held with forceps, demonstrating its translucent, orange-tinted appearance and self-supporting structural integrity following gelation.

4.2 Rheological Analysis

In viscoelasticity, the storage modulus G’ and loss modulus G” quantify how a material balances solid-like elasticity and liquid-like viscosity under stress. The storage modulus G’ measures the elastic behavior,

representing the energy stored and fully recovered during each deformation cycle. A high G’ value indicates a rigid, stiff, or rubbery structure that acts like a mechanical spring and returns to its original shape. Conversely, the loss modulus G” measures the viscous behavior, representing the energy lost or dissipated as heat during deformation. A high G” value signifies a more fluid-like structure that flows, yields, and permanently absorbs energy under stress. By comparing these two values, it is possible to determine the overall state of a material; when G’ is greater than G”, the material behaves predominantly like an elastic solid, whereas when G” is greater than G’, it behaves more like a viscous liquid. To determine G’ and G”, rheological tests were performed. Running an oscillatory rheometer test enables the decoupling of G’ and G” by applying a controlled sinusoidal twisting stress to a material and measuring the resulting strain. In a viscoelastic material, the strain response lags behind the stress by a specific phase angle, δ. An amplitude sweep and a frequency sweep serve as a sequential two-step process to map out these properties accurately.

4.2.1 Amplitude Sweep — Mechanical Characterization and Comparison of Hydrogel Systems

Beginning with the PEGDA hydrogels, when examining the oscillatory amplitudes sweeps, G’ remained fairly stable and was staying well above G” throughout the low strain plateau region, which extended to approximately 0.5 - 1 % strain (Figure 4.5). In this region, G’ surpasses G” by approximately one order of magnitude, a consistent indicator of a predominantly elastic network. Once the applied strain went beyond the LVR, G’ progressively decreased, indicating that the hydrogel network was starting to break down and yield under the increasing mechanical strain.

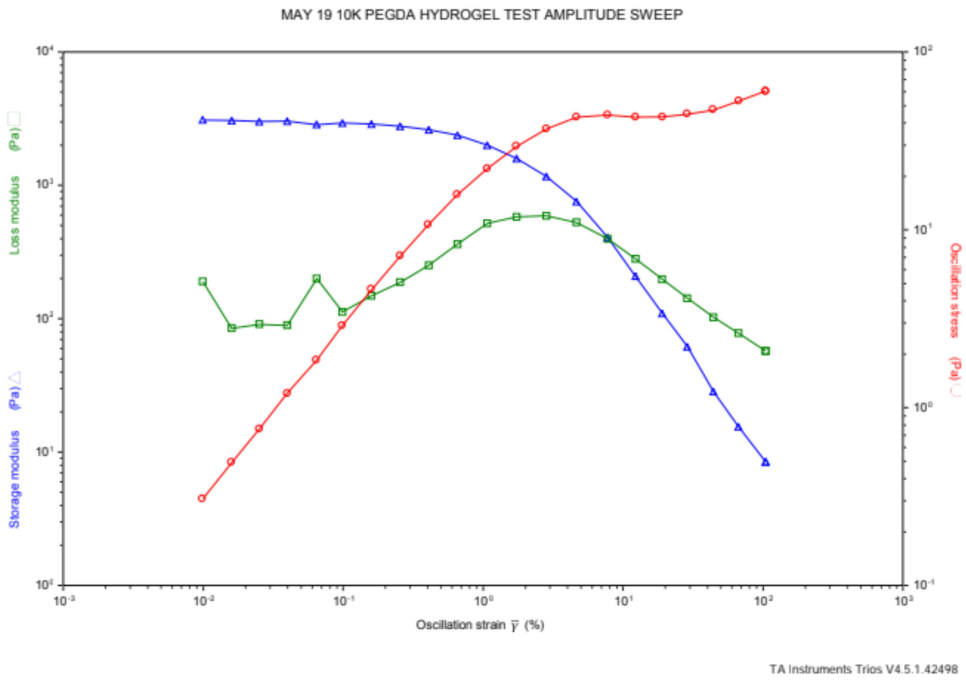

Figure 4.5 - Oscillatory amplitude sweep of the PEGDA hydrogel. Storage modulus G′ (blue triangles) and loss modulus G″ (green squares) are plotted as a function of oscillation strain (%) at a fixed frequency of 1.0 Hz and 25°C. The red circles represent oscillation stress (right y-axis). G′ remains constant and dominant over G″ throughout the low-strain plateau region, defining the linear viscoelastic region (LVR) up to approximately 0.5 -1% strain, beyond which G′ decreases progressively, indicating the onset of network yielding.

As for the PEG-propionaldehyde/PEG-amine viscoelastic hydrogel, a stable LVR was similarly identified at low strains, with G′ remaining constant and greater than G″ up to approximately 10 - 50% strain (Figure 4.6). Notably, the separation between G′ and G″ within the LVR was considerably smaller than that observed for PEGDA, with G′ exceeding G″ by roughly half an order of magnitude. This narrowed separation between the two moduli is an initial indicator of the greater viscous contribution present in the viscoelastic hydrogel network relative to the purely elastic PEGDA control. A strain of 1% was selected as the fixed strain for all subsequent frequency sweep measurements for both hydrogel systems, as this value fell well within the LVR of both materials.

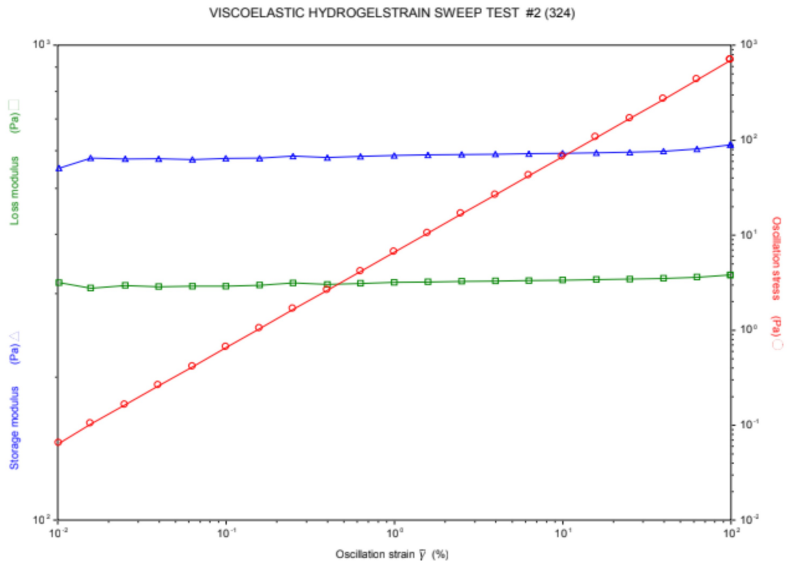

Figure 4.6 - Oscillatory amplitude sweep of the PEG-propionaldehyde/PEG-amine viscoelastic hydrogel. Storage modulus G′ (blue triangles) and loss modulus G″ (green squares) are plotted as a function of oscillation strain (%) at a fixed frequency of 1.0 Hz and 25°C. The red circles represent oscillation stress (right y-axis). G′ remains constant and greater than G″ throughout an extended LVR up to approximately 10-50% strain. The reduced separation between G′ and G″ compared to the PEGDA control is indicative of the greater viscous contribution present within the viscoelastic hydrogel network.

4.2.2 Frequency Sweep — Mechanical Characterization and Comparison of Hydrogel Systems

Rheological characterization via frequency sweep analysis demonstrates that the PEGDA hydrogel exhibits a storage modulus of (G′) of approximately 1,500-2,000 Pa that did not vary across the angular frequency range of 0.1 - 100 Hz (Figure 4.7). No crossover between G' and G" was seen at any point of this test, signifying the absence of a sol-gel transition or structural relaxation. G' overall maintained a stable plateau up to around 20 Hz, where a drop in G' could be seen; however, this sudden drop is not a true property of the material, but rather is attributed to inertial and compliance limitations of the rheometer transducer rather than intrinsic material behavior. The dominance of G' over G" across the tested frequency domain confirms that the permanent covalent crosslinking network imparts a time-independent, predominantly elastic solid state to the PEGDA hydrogel.

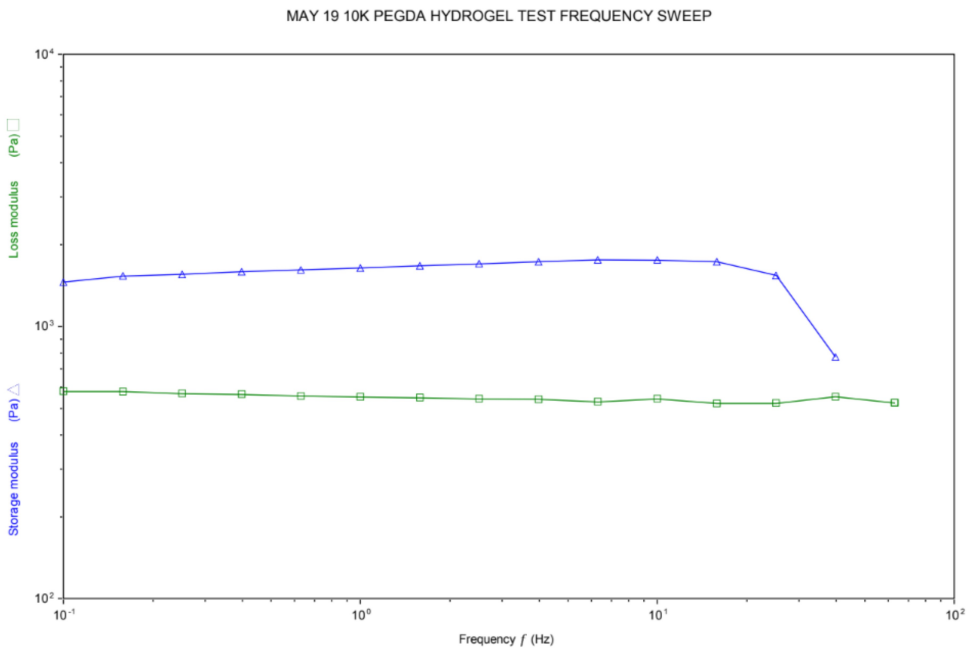

Figure 4.7 - Oscillatory frequency sweep of the PEGDA hydrogel. Storage modulus G′ (blue triangles) and loss modulus G″ (green squares) are plotted as a function of frequency (Hz) at a fixed strain of 1% and 25°C. G′ remains flat and dominant over G″ across the entire frequency range tested, with no observable G′/G″ crossover, confirming the frequency-independent, purely elastic mechanical behavior characteristic of a permanently covalently crosslinked polymer network. The decrease in G′ observed above approximately 20 Hz is attributed to instrument inertia artifacts at high deformation rates.

Conversely, when examining the frequency sweep of the PEG-propionaldehyde/PEG-amine hydrogel, it revealed a significantly more intricate viscoelastic profile than the PEGDA hydrogel (Figure 4.8). At lower angular frequencies (~0.1 - 0.3 rad/s), the loss modulus (G") surpassed the storage modulus (G'), indicating that the material behaved in a mainly viscous, liquid-like manner over longer deformation timescales. A crossover between G' and G", indicative of a sol-gel transition or structural relaxation, can be seen at approximately 0.3-0.5 rad/s, past which G′ exceeds G″, and both moduli increased as a function of frequency. At higher frequencies, the hydrogel responded in an increasingly elastic, solid-like manner, which was attributable to the restricted relaxation kinetics as the polymer chains and dynamic crosslinks had insufficient time to rearrange on the timescale of the applied deformation.

This cross over between G’ and G” is the clearest quantitative evidence that the material is viscoelastic, and it is a behavior that was not observed in the elastic-dominant PEGDA graphs. The frequency at which this crossover happens also gives an estimate of how quickly the hydrogel network can rearrange itself, more specifically how fast the network, governed by dynamic imine crosslinks and physical chain

entanglement, is expected to shift and dissipate stress. The fact that both G′ and G″ change with frequency, combined with the crossover at low frequencies, confirms that the PEG-propionaldehyde/PEG-amine hydrogel is a true viscoelastic material. This finding is also consistent with the qualitative behavior observed during inversion creep testing, where the hydrogel was seen to slowly flow and deform under gravity over time.

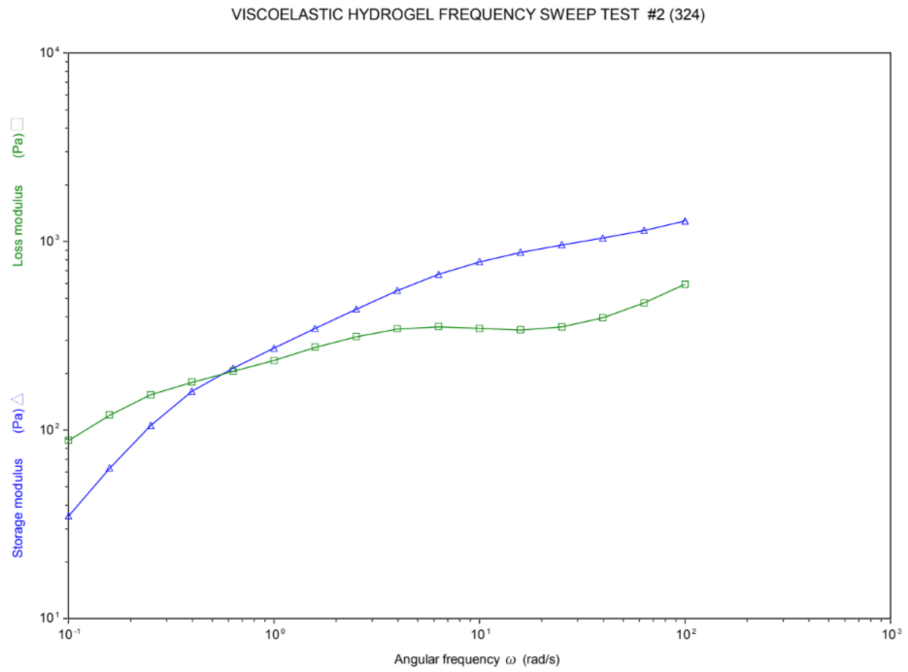

Figure 4.8 - Oscillatory frequency sweep of the PEG-propionaldehyde/PEG-amine viscoelastic hydrogel. Storage modulus G′ (blue triangles) and loss modulus G″ (green squares) are plotted as a function of angular frequency (rad/s) at a fixed strain of 1% and 25°C. At low angular frequencies (~0.1-0.3 rad/s), G″ exceeds G′, indicating liquid-like, viscous-dominant behavior over long timescales. A G′/G″ crossover is observed at approximately 0.3-0.5 rad/s, above which G′ rises above G″ and both moduli increase continuously with frequency, reflecting elastic-dominant behavior at short timescales. This frequency-dependent response and low-frequency crossover confirm the viscoelastic nature of the hydrogel network.

This frequency-dependent behavior stands in direct contrast to the flat, frequency-independent response observed for PEGDA and is the hallmark mechanical signature of a viscoelastic material. The observed increase in both moduli with frequency is consistent with the presence of dynamic relaxation mechanisms within the polymer network. At high frequencies, the polymer chains and dynamic imine crosslinks do not have sufficient time to rearrange, causing the material to respond more elastically. At lower frequencies, these network rearrangements occur on the timescale of the applied deformation, allowing the material to

partially dissipate stress and exhibit greater viscous behavior. This timescale-dependent mechanical response is precisely what distinguishes viscoelastic hydrogels from their purely elastic counterparts and is consistent with the intended dynamic nature of the imine crosslinks and physical chain entanglements within this hydrogel system.

4.3 Degradation tests

Two distinct behaviors occurred during the degradation tests and this depended on either hydrogel age or temperature conditions. The two behaviors consist of progressive degradation leading to the hydrogel being completely dissolved or progressive swelling.

The newest three hydrogels, which were gelated 6 days prior to the tests, exhibited degradation. The two hydrogels that were stored at -20°C (Gel 4, Gel 5) displayed a steady decrease in mass beginning almost immediately once they were slightly submerged in PBS. These hydrogels decreased to 60.7% and 66.3% of initial mass by the 70 minute point, before fully dissolving at the 85 and 95 minute point. The last hydrogel in this group, which was transferred to room temperature for four days prior to testing (Gel 6), showed an initial gain in mass (102.1% at the 10 minute point) followed by a slightly more gradual decrease than its frozen counterparts. This hydrogel reached 92.2% of its initial mass at 70 minutes and ended up dissolving at the 165 minute mark.

In contrast, the last three hydrogels did not degrade, but instead they progressively gained mass, with Gel 1, Gel 2 and Gel 3 increasing to 138.1%, 126.2% and 122.7% of their initial mass by the 70 minute mark. Due to the fact that these hydrogels were not degrading in any way, intermediate weight measurements were not logged until the very end when the room temperature hydrogel from the first group was last weighted (165 minutes). Gel 1 had a total increase of 152.9% of its initial mass, and both Gel 2 and Gel 3 increased to 134.9% and 133.1% from their initial masses.

Table 4.1: Summary of hydrogel fabrication dates, storage conditions, and age at degradation testing.

Hydrogel	Storage Temperature	Age at Testing
Gel 1	22.7°C	3 months

Gel 2	22.7°C	15 days
Gel 3	22.7°C	15 days
Gel 4	−20°C	6 days
Gel 5	−20°C	6 days
Gel 6	-20ºC → 21°C	6 days (4 days at 21°C)

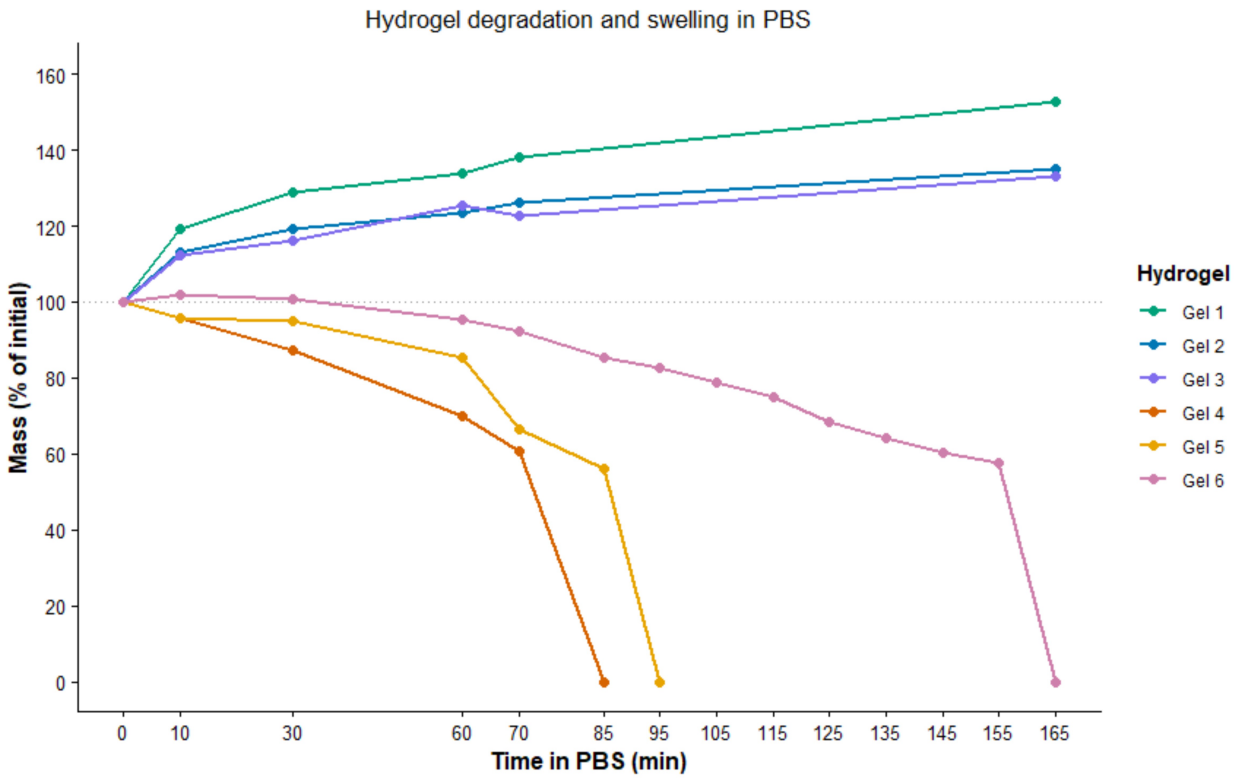

Figure 4.9 - Hydrogel degradation and swelling behavior in PBS over time. The wet weight of six PEG-propionaldehyde/PEG-amine hydrogels was measured over time. Weight changes are reported as a percentage of initial weight. Gels 4, 5 and Gel 6 showed progressive mass loss and were fully dissolved by 95 and 165 minutes, respectively. Gels 1,2, and 3 showed no degradation within the testing window and instead progressively swelled, gaining mass throughout testing.

CHAPTER 5. Discussion

The combined qualitative and quantitative data show that combining PEG-propionaldehyde and PEG-amine successfully formed a viscoelastic PEG hydrogel. This hydrogel showed distinct mechanical properties when compared to the purely elastic control PEGDA hydrogel. These results are consistent with physical entanglement and dynamic imine crosslinks jointly contributing to viscoelasticity in synthetic PEG networks, without requiring complex chemistries [63,73].

Both hydrogels showed a stable LVR in strain sweeps, where the storage modulus (G') remained constant and much higher than the loss modulus (G"). The PEGDA hydrogel had an LVR up to approximately 0.5-1% strain, with G' one order of magnitude above G", representative of a stiff elastic network. The PEG-propionaldehyde/PEG-amine hydrogel kept a stable LVR up to approximately 10-50% strain, with G' higher than G" . For the viscoelastic hydrogel, the values of G’ and G” were closer together, separated by about a half an order of magnitude. This reduced distance between G' and G" indicates more viscous behavior than the PEGDA hydrogel control, likely because dynamic crosslinks and physically entangled polymer chains allow the network to dissipate some energy under small strains[53]. Neither material showed a yield point during testing. This proves that both networks formed well and confirms that a 1% strain was an appropriate choice for the LVR in frequency sweep experiments.

Frequency sweep results reveal distinct mechanical differences between the two hydrogels, highlighting a clear contrast between a purely elastic network and a highly dynamic viscoelastic matrix. The PEGDA hydrogel shows a stable storage modulus (G’) of 1,500 - 2,000 Pa across the entire frequency range of 0.1 - 100 Hz. Throughout this tested range, G' remains constant and consistently higher than the loss modulus (G"), with no crossover behavior observed. This pronounced elastic plateau confirms the formation of a permanently covalently crosslinked elastic that reacts uniformly regardless of the deformation speed.. Notably, the decline in G′ observed above approximately 20 Hz can be attributed to instrument inertia at high deformation rates and does not reflect the material property of the material [77].

In contrast, the frequency sweep results of the PEG-propionaldehyde/PEG-amine hydrogel demonstrate a strong frequency dependence that confirms true viscoelastic behavior. At low angular frequencies

between 0.1-0.3 rad/s, G″ surpasses G′, indicating that the material behaved as a viscous liquid over long timescales. A distinct G′/G″ crossover was observed at approximately 0.3-0.5 rad/s, above which G′ rises above G″, and both moduli increase continuously with frequency, reflecting increasingly elastic, solid-like behavior at short timescales. This crossover frequency defines the characteristic relaxation timescale of the network, which is expected to reflect rearrangement of dynamic imine crosslinks and entangled polymer chains, though this study did not isolate their individual contributions [53]. Consequently, fast deformations above this frequency trigger an elastic response, whereas slow deformations below it allow network rearrangements and viscous dissipation to dominate [53], validating the intended viscoelastic design.

These quantitative findings are reinforced by the qualitative inversion tests and macroscopic flow behavior observed during characterization. Upon inversion, the hydrogel initially maintained its shape, exhibiting solid-like behavior over short timescales; however, over extended periods, it slowly flowed along the test tube walls and eventually spread into a disc-like layer when placed in a petri dish. This macroscopic creep behavior is consistent with the low-frequency G″ dominance observed during frequency sweeps, where the material behaves as a viscoelastic liquid over long timescales. The subsequent G′/G″ crossover at higher frequencies, where G′ becomes dominant, reflects the solid-like behavior observed over short timescales. Together, these results confirm that the material exhibits the defining hallmarks of a viscoelastic material, with its liquid-like or solid-like character depending on the timescale of observation [53].

Furthermore, degradation/swelling tests further provide insight into the time- and temperature-dependent character of this hydrogel system. Freshly prepared hydrogels held at -20°C for 6 days degraded rapidly upon PBS exposure, dissolving completely within 85 - 95 minutes. In contrast, hydrogels from the same formulation batch that were transitioned from -20ºC to 21°C following 2 days in cold storage and held at 21ºC 4 days prior to testing exhibited a more gradual breakdown and survived significantly longer before fully dissolving. These observations suggest that the polymer network does not reach a fully matured state immediately following initial gelation. Aging at 21°C likely allows the constituent polymer chains sufficient time to form additional physical entanglements and/or establish a higher density of imine bonds,

thereby rendering the network more resistant to hydrolytic or physical breakdown [78]. This mechanism is highly consistent with earlier qualitative observations described earlier in this thesis, which noted that hydrogels held at -20°C for several days were noticeably firmer than those evaluated immediately after gelation.

Hydrogels aged at 21°C for extended periods (15+ days) displayed a distinct behavior, absorbing the PBS and gaining over 20% of their initial mass within 70 mins. This suggests that the balance between degrading and swelling in this hydrogel system depends on the amount of time the hydrogel is permitted to mature: less aged networks are more susceptible to degradation and dissolution, while longer aged networks behave more like a nondegradable hydrogel that retains its structure while absorbing solvent. Given that dynamic imine bonds are inherently reversible, it is possible that continued aging allows the polymer network to settle into a more highly entangled and/or more extensively crosslinked configuration that is less prone to dissolution in an aqueous solution, while remaining highly hydrophilic and water-absorbing [73].

These findings have implications for the practical use of this material and illustrate what future steps should be. Because the degree of network maturation strongly affects gel stability in aqueous environments, any future work intending to use this hydrogel as a cell scaffold must first conduct longer term studies with the hydrogel immersed. Additionally, it is necessary to assess the mechanical properties of a fully swollen gel.. In addition, for purposes other than cell culture, the time-dependent maturation of this hydrogel could itself be used as a tunable design parameter. For example, it may be possible to engineer a hydrogel with a predictable, controlled dissolution window for time-released delivery applications [79], as will be discussed further in Chapter 7.

One limitation of the current study is that longer term swelling/degradation studies were not performed. Future studies could evaluate this on the order of days-weeks-months. In addition, the strain sweep did not extend to the yield point of either hydrogel, preventing a precise pinpoint of the critical strain where the polymer network fails. Future studies should consist of extending the strain range to fully characterize the yield behavior and to better understand the mechanical limits of both hydrogels Additionally,, direct stress relaxation experiments should be performed to quantify relaxation time constants and to distinguish

the proportion of the viscoelastic response due from physical entanglement and that due to reversible imine bond exchange. Because imine bond exchange is a chemically activated process, its relaxation rate is highly temperature-dependent. By measuring the relaxation time constant τ at different temperatures, the chemical exchange will reveal the proportion due to the imine bond exchange.. Conversely, the relaxation of entanglements is driven by chain mobility. Above the glass transition temperature, this process obeys standard polymer melt dynamics.

While the motivation for this thesis was to develop a viscoelastic scaffold for RPE cells, this was the first step in a series of several steps towards that goal. For instance, at present, the viscoelastic hydrogel completely dissolves in tissue culture conditions (e.g., media at 37ºC; data not shown). Both the Bruch's membrane as well as the subretinal extracellular matrix are both viscoelastic in nature, and stiffening due to old age and any overall changes to their time dependent properties have shown to impair and or damage RPE cell function [25,51]. Given that RPE cells are known to be highly sensitive to viscoelastic substrate cues [49,51], a viscoelastic hydrogel may more accurately mimic the mechanical environment that RPE cells experience in vivo compared to an elastic hydrogel. The ability to incorporate viscoelastic behavior into a synthetic PEG hydrogel without dependence on complex supramolecular assemblies or dynamic covalent chemistries signifies a meaningful step forward for the field of tissue engineering.

CHAPTER 6. Conclusion

This thesis establishes that a simple PEG-propionaldehyde/PEG-amine formulation can produce a hydrogel with mechanical behavior fundamentally different from that of a conventionally crosslinked elastic PEG network. Rather than maintaining the same mechanical response across deformation timescales, the resulting hydrogel transitioned between viscous-dominant and elastic-dominant behavior depending on the frequency of deformation. Together with its time-dependent macroscopic flow, this behavior demonstrates that the material possesses a dynamic polymer network capable of rearrangement on experimentally relevant timescales. An important outcome of this work is that the hydrogel cannot be described by a single stiffness value. Its mechanical state depends on both the timescale over which it is

interrogated and the history of the material after gelation. The unexpected transition from rapid dissolution in relatively young hydrogels to substantial swelling without dissolution in more mature hydrogels suggests that network formation continues after the initial gelation period. Thus, hydrogel age and storage history are material parameters that may be as important as polymer composition in determining the final properties of this system.

These findings also refine the original premise of the project. The goal was to develop a synthetic viscoelastic material that could ultimately serve as a mechanically relevant scaffold for retinal pigment epithelial cells. The present work establishes the material basis required to pursue that goal, but it also demonstrates that viscoelasticity alone is insufficient to define a useful scaffold. A successful material must combine an appropriate time-dependent mechanical response with predictable stability, swelling, transport, geometry, and biological functionality under physiological conditions.

Accordingly, the principal contribution of this thesis is the identification of a PEG-based formulation that provides a working starting point for engineering those properties. The observed rheological behavior is consistent with the intended network design, in which reversible imine bond formation and physical chain entanglement were expected to jointly govern stress relaxation. However, this study did not directly confirm imine bond formation (e.g., via FTIR or NMR) or independently quantify the degree of chain entanglement, so the relative contribution of each mechanism to the observed viscoelasticity remains inferred rather than directly demonstrated. Establishing that relationship will make it possible to move from demonstrating viscoelasticity to deliberately engineering it. In this way, the work presented here provides the foundation for developing a tunable synthetic platform in which time-dependent mechanics can eventually be isolated as a design variable and used to determine how viscoelasticity influences RPE behavior.

CHAPTER 7. Future Directions

The next stage of this work should shift from demonstrating that the PEG-propionaldehyde/PEG-amine hydrogel is viscoelastic to establishing control over its viscoelastic behavior. Ultimately, the value of this system will depend on whether its mechanical properties can be predictably engineered and maintained

under physiological conditions. Future studies should therefore focus on defining the relationships among network chemistry, polymer entanglement, material aging, viscoelasticity, and biological response.

7.1 Establish the mechanism and design rules governing viscoelasticity

A central unanswered question is how much of the observed viscoelastic response arises from reversible imine bond exchange and how much arises from physical entanglement of the PEG chains. The experiments in this thesis demonstrate the resulting macroscopic behavior but do not distinguish the relative contributions of these mechanisms. Future studies should systematically vary parameters expected to affect them differently, including polymer molecular weight, polymer concentration, functional-group stoichiometry, temperature, and gel maturation time. Direct stress-relaxation and creep-recovery measurements should accompany frequency sweeps so that characteristic relaxation times can be quantified rather than inferred solely from crossover behavior. These experiments would allow the current formulation to become a tunable material system. Instead of determining whether the hydrogel is viscoelastic, subsequent studies could determine how specific changes in network structure shift relaxation time, storage and loss moduli, swelling, and resistance to dissolution. This would establish design rules for independently controlling the properties most relevant to a tissue-engineering scaffold.

7.2 Control network maturation and physiological stability

The strong dependence of hydrogel stability on material age suggests that network maturation is an important feature of this system rather than simply an experimental complication. A systematic aging study should therefore characterize hydrogels at defined intervals after initial gelation and determine how their rheological properties, swelling, and dissolution behavior evolve with time. These studies should be conducted under physiologically relevant conditions, particularly at 37°C in cell culture medium, because stability under those conditions is required before meaningful cell studies can be performed. If maturation alone cannot provide sufficient stability, a secondary stabilization mechanism could be introduced. Partial permanent crosslinking is one possibility, but it should be used as a controlled design variable rather than simply as a means of preventing dissolution. Increasing permanent crosslink density would be expected to alter the same stress-relaxation behavior that makes the material of interest. The appropriate

formulation would therefore be one that provides sufficient structural persistence for cell culture while preserving a measurable and tunable viscoelastic response.

7.3 Develop a mechanically defined platform for RPE mechanobiology

Once stable formulations are established, the most important biological question is whether RPE cells respond differently to substrate viscoelasticity when other material properties are controlled. This requires more than comparing the current viscoelastic hydrogel with PEGDA because the two materials differ in multiple characteristics in addition to viscoelasticity. A stronger experimental platform would consist of a family of PEG hydrogels with similar initial stiffness, ligand density, geometry, and surface chemistry but different relaxation behaviors. RPE cells cultured on these mechanically defined substrates could then be evaluated for attachment, spreading, polarization, monolayer formation, viability, and RPE-specific functions. Such experiments would directly test the premise motivating this thesis: whether time-dependent mechanics are an independent regulator of RPE phenotype. They could also determine whether there is an optimal range of stress-relaxation behavior that supports RPE function rather than assuming that greater viscoelasticity is necessarily beneficial. This approach would be particularly valuable for modeling age-related macular degeneration. Rather than developing a single material intended to represent Bruch's membrane, a tunable PEG platform could be used to reproduce different mechanical states associated with healthy and aged tissue. The system could therefore serve both as a potential scaffold-development platform and as an in vitro model for investigating how changes in extracellular matrix mechanics contribute to RPE dysfunction.

7.4 Extend the material platform beyond retinal tissue engineering

The time-dependent dissolution and swelling observed in this study may also provide opportunities outside the original retinal application. If network maturation and relaxation can be predictably controlled, the same material parameters could potentially be used to regulate retention and release of incorporated molecules. This possibility should be investigated only after the underlying network behavior has been quantitatively defined, since predictable drug delivery requires reproducible relationships among network structure, swelling, dissolution, and molecular transport. More broadly, a synthetic PEG system in which

viscoelasticity can be systematically varied would have utility beyond RPE cells. Many cell types respond to the time-dependent mechanics of their extracellular matrix. Establishing control over this relatively simple hydrogel system could therefore provide a general experimental platform for separating the effects of matrix stiffness from stress relaxation and investigating how cells interpret dynamic mechanical environments.

REFERENCES

1. Vyawahare, H., & Shinde, P. (2022). Age-related macular degeneration: Epidemiology, pathophysiology, diagnosis, and treatment. *Cureus*, 14(9), e29583.

2. Ambati, J., & Fowler, B. J. (2012). Mechanisms of age-related macular degeneration. *Neuron*, 75(1), 26–39.

3. Ingram, N. T., Fain, G. L., & Sampath, A. P. (2020). Elevated energy requirement of cone photoreceptors. *PNAS*, 117(32), 19599–19603. PMID: 32719136.

4. Anderson, D. H., Talaga, K. C., Rivest, A. J., Barron, E., Hageman, G. S., & Johnson, L. V. (2004). Characterization of beta amyloid assemblies in drusen: the deposits associated with aging and age-related macular degeneration. Experimental Eye Research, 78(2), 243–256. So

5. Belgio, B., Boschetti, F., & Mantero, S. (2021). Towards an in vitro retinal model to study and develop new therapies for age-related macular degeneration. *Bioengineering*, 8(2), 18.

6. Wang, L., & Mao, X. (2021). Role of retinal amyloid-β in neurodegenerative diseases: Overlapping mechanisms and emerging clinical applications. *International Journal of Molecular Sciences*, 22(5), 2360. PMID: 33652721.

7. Bhutto, I., & Lutty, G. (2012). Understanding age-related macular degeneration (AMD). *Molecular Aspects of Medicine*, 33(4), 295–317.

8. Cheng, S., Zhang, S., Huang, M., Liu, Y., Zou, X., Chen, X., & Zhang, Z. (2024). Treatment of neovascular age-related macular degeneration with anti-VEGF drugs. *Frontiers in Medicine*, 11, 1411278.

9. Wong, W. L., Su, X., Li, X., Cheung, C. M. G., Klein, R., Cheng, C. Y., & Wong, T. Y. (2014). Global prevalence of age-related macular degeneration and disease burden projection for 2020 and 2040: a systematic review and meta-analysis. *The Lancet Global Health*, 2(2), e106–e116. PMID: 25104651.

10. Si, Z., Zheng, Y., & Zhao, J. (2023). The role of retinal pigment epithelial cells in age-related macular degeneration: Phagocytosis and autophagy. *Biomolecules*, 13(6), 901. PMID: 37371481.

11. Discher, D. E., Janmey, P., & Wang, Y. L. (2005). Tissue cells feel and respond to the stiffness of their substrate. *Science*, 310(5751), 1139–1143.

12. Egbowon, B. F., Fornari, E., Pally, J. M., Hargreaves, A. J., Stevens, B., McGinnity, T. M., & Pierscionek, B. K. (2023). Retinal pigment epithelial cells can be cultured on fluocinolone acetonide-treated nanofibrous scaffold. *Materials & Design*, 232, 112152.

13. Fleckenstein, M., Schmitz-Valckenberg, S., & Chakravarthy, U. (2024). Age-related macular degeneration: A review. *JAMA*, 331(2), 147–157. PMID: 38193957.

14. Gandhi, J. K., Manzar, Z., Bachman, L. A., Andrews-Pfannkoch, C., Knudsen, T., Hill, M., Schmidt, H., Iezzi, R., Pulido, J. S., & Marmorstein, A. D. (2018). Fibrin hydrogels as a xenofree and rapidly degradable support for transplantation of retinal pigment epithelium monolayers. *Acta Biomaterialia*.67, 134–146.

15. Gandhi, J. K., et al. (2020). Fibrin hydrogels are safe, degradable scaffolds for sub-retinal implantation. *PLOS ONE*, 15(1), e0227641.

16. Hersel, U., Dahmen, C., & Kessler, H. (2003). RGD modified polymers: Biomaterials for

stimulated cell adhesion and beyond. *Biomaterials*, 24(24), 4385–4415.

17. Hoh Kam, J., Lenassi, E., & Jeffery, G. (2010). Viewing ageing eyes: Diverse sites of amyloid beta accumulation in the ageing mouse retina. *PLOS ONE*, 5(10), e13127.

18. Lakkaraju, A., Umapathy, A., Tan, L. X., Daniele, L., Philp, N. J., Boesze-Battaglia, K., & Williams, D. S. (2020). The cell biology of the retinal pigment epithelium. *Progress in Retinal and Eye Research*, 78, 100846. PMID: 32105772.

19. Lee, I., Xie, R., Luz-Madrigal, A., Min, S., Zhu, J., Jin, J., Edwards, K. L., Phillips, M. J., Ludwig, A. L., Gamm, D. M., Gong, S., & Ma, Z. (2023). Micromolded honeycomb scaffold design to support the generation of a bilayered RPE and photoreceptor cell construct. *Bioactive Materials*, 30, 142–153.

20. Lutolf, M. P., Lauer-Fields, J. L., Schmoekel, H. G., Metters, A. T., Weber, F. E., Fields, G. B., & Hubbell, J. A. (2003). Synthetic matrix metalloproteinase-sensitive hydrogels for the conduction of tissue regeneration. *PNAS*, 100(9), 5413–5418.

21. Majidnia, E., Ahmadian, M., Salehi, H., & Amirpour, N. (2022). Development of an electrospun poly(ε-caprolactone)/collagen-based human amniotic membrane powder scaffold for culturing retinal pigment epithelial cells. *Scientific Reports*, 12(1), 6469.

22. Masland, R. H. (2012). The neuronal organization of the retina. *Neuron*, 76(2), 266–280.

23. Pennington, K. L., & DeAngelis, M. M. (2016). Epidemiology of age-related macular degeneration (AMD): associations with cardiovascular disease phenotypes and lipid factors. Eye and Vision, 3, 34.

24. Ferris, F. L., III, Wilkinson, C. P., Bird, A., Chakravarthy, U., Chew, E., Csaky, K., Sadda, S. R., & Beckman Initiative for Macular Research Classification Committee. (2013). A clinical classification for age-related macular degeneration. *Ophthalmology, 120*(4), 844–851.

25. Rickabaugh, E., Weatherston, D., Harris, T. I., Jones, J. A., & Vargis, E. (2023). Engineering a biomimetic in vitro model of Bruch's membrane using hagfish slime intermediate filament proteins. *ACS Biomaterials Science & Engineering*, 9(8), 5051–5061.

26. Rizzolo, L. J., Nasonkin, I. O., & Adelman, R. A. (2022). Retinal cell transplantation, biomaterials, and in vitro models for developing next-generation therapies of age-related macular degeneration. *Stem Cells Translational Medicine*, 11(3), 269–281.

27. Rosenfeld, P. J., Brown, D. M., Heier, J. S., Boyer, D. S., Kaiser, P. K., Chung, C. Y., & Kim, R. Y. (2006). Ranibizumab for neovascular age-related macular degeneration. *The New England Journal of Medicine*, 355(14), 1419–1431.

28. Shadforth, A. M. A., George, K. A., Kwan, A. S., Chirila, T. V., & Harkin, D. G. (2012). The cultivation of human retinal pigment epithelial cells on Bombyx mori silk fibroin. *Biomaterials*, 33(16), 4110–4117.

29. Strauss, O. (2005). The retinal pigment epithelium in visual function. *Physiological Reviews*, 85(3), 845–881.

30. Falavarjani, K. G., & Nguyen, Q. D. (2013). Adverse events and complications associated with intravitreal injection of anti-VEGF agents: A review of literature. *Eye*, 27(7), 787–794.

31. Wei, Y., Alexandre, U., & Ma, X. (2022). Hydrogels to support transplantation of human embryonic stem cell-derived retinal pigment epithelial cells. *Brain Sciences*, 12(12), 1620.

32. Wu, K. Y., Qian, S. Y., Camiré, A., Kim, D. T., & Giunta, M. (2025). Aflibercept for Wet Age-

Related Macular Degeneration: A Prospective, Randomized Trial Comparing Treat-And-Extend and Fixed Bimonthly Dosing. *Journal of Clinical Medicine*, 14(22), 8180.

33. Zimmermann, J. A., Irlenbusch, L., Hansen, U., Himmler, M., Zeng, C., Eter, N., Fuchsluger, T., & Heiduschka, P. (2025). Long-term cultivation of retinal pigment epithelium cells on nanofiber scaffolds. *Graefe's Archive for Clinical and Experimental Ophthalmology*, 263, 1327–1336.

34. Garg, S. J., & Hadziahmetovic, M. (2024). Verteporfin photodynamic therapy for the treatment of chorioretinal conditions: A narrative review. *Clinical Ophthalmology*, 18, 1701–1716.

35. Csaky, K. G., Miller, J. M. L., Martin, D. F., & Johnson, M. W. (2024). Drug approval for the treatment of geographic atrophy: How we got here and where we need to go. *American Journal of Ophthalmology*, 263, 231–239.

36. Cruz-Pimentel, M., & Wu, L. (2023). Complement inhibitors for advanced dry age-related macular degeneration (geographic atrophy): Some light at the end of the tunnel? *Journal of Clinical Medicine*, 12(15), 5131.

37. Li, Z., Hu, Z., & Gao, Z. (2025). Advances in the study of age-related macular degeneration based on cell or cell-biomaterial scaffolds. *Bioengineering*, 12(3), 278.

38. Marcos, L. F., Wilson, S. L., & Roach, P. (2021). Tissue engineering of the retina: From organoids to microfluidic chips. *Journal of Tissue Engineering*, 12.

39. Hampton, C., Bharti, K., & Song, M. J. (2024). Tissue engineering of outer blood retina barrier for therapeutic development. *Current Opinion in Biomedical Engineering*, 31, 100538.

40. Dujardin, C., Habeler, W., Monville, C., Letourneur, D., & Simon-Yarza, T. (2023). Advances in the engineering of the outer blood-retina barrier: From in-vitro modelling to cellular therapy. *Bioactive Materials*, 31, 151–177.

41. Galloway, C. A., Dalvi, S., Shadforth, A. M. A., Suzuki, S., Wilson, M., Kuai, D., Hashim, A., MacDonald, L. A., Gamm, D. M., Harkin, D. G., & Singh, R. (2018). Characterization of human iPSC-RPE on a prosthetic Bruch's membrane manufactured from silk fibroin. *Investigative Ophthalmology & Visual Science*, 59(7), 2792–2800.

42. Shadforth, A. M., Suzuki, S., Alzonne, R., Edwards, G. A., Richardson, N. A., Chirila, T. V., & Harkin, D. G. (2015). Incorporation of human recombinant tropoelastin into silk fibroin membranes with the view to repairing Bruch's membrane. *Journal of Functional Biomaterials*, 6(3), 946–962.

43. Oleksy, M., Dynarowicz, K., & Aebisher, D. (2023). Advances in biodegradable polymers and biomaterials for medical applications: A review. *Molecules*, 28(17), 6213.

44. Lin, C.-C., & Anseth, K. S. (2009). PEG hydrogels for the controlled release of biomolecules in regenerative medicine. *Pharmaceutical Research*, 26(3), 631–643.

45. Chaudhuri, O., Gu, L., Klumpers, D., Darnell, M., Bencherif, S. A., Weaver, J. C., Huebsch, N., Lee, H.-P., Lippens, E., Duda, G. N., & Mooney, D. J. (2016). Hydrogels with tunable stress relaxation regulate stem cell fate and activity. *Nature Materials*, 15(3), 326–334.

46. Chaudhuri, O., et al. (2015). Substrate stress relaxation regulates cell spreading. *Nature Communications*, 6, 6364.

47. Crandell, P., & Stowers, R. (2023). Spatial and temporal control of 3D hydrogel viscoelasticity through phototuning. *ACS Biomaterials Science & Engineering*, 9(12), 6860–6869.

48. Lai, W., Geliang, H., Bin, X., & Wang, W. (2025). Effects of hydrogel stiffness and viscoelasticity on organoid culture: A comprehensive review. *Molecular Medicine*, 31, 83.

49. Ciccone, G., Azevedo Gonzalez-Oliva, M., Versaevel, M., Cantini, M., Vassalli, M., Salmeron-Sanchez, M., & Gabriele, S. (2025). Epithelial cell mechanoresponse to matrix viscoelasticity and confinement within micropatterned viscoelastic hydrogels. *Advanced Science*, 12(18), 2408635.

50. Thekkethil, N., Köry, J., Guo, M., Stewart, P. S., Hill, N. A., & Luo, X. (2024). Modelling the rheology of living cell cytoplasm: Poroviscoelasticity and fluid-to-solid transition. *Biomechanics and Modeling in Mechanobiology*, 23(5), 1551–1569.

51. Wolfram, L., Gimpel, C., Schwämmle, M., Clark, S. J., Böhringer, D., & Schlunck, G. (2024). The impact of substrate stiffness on morphological, transcriptional and functional aspects in RPE. *Scientific Reports*, 14(1), 7488.

52. Hoffman, A.S. (2002). Hydrogels for biomedical applications. *Advanced Drug Delivery Reviews*, 54(1), 3–12. PMID: 11755703.

53. Chaudhuri, O., Cooper-White, J., Janmey, P. A., Mooney, D. J., & Shenoy, V. B. (2020). Effects of extracellular matrix viscoelasticity on cellular behaviour. *Nature*, 584, 535–546.

54. Lou, J., Stowers, R., Nam, S., Xia, Y., & Chaudhuri, O. (2018). Stress relaxing hyaluronic acid-collagen hydrogels promote cell spreading, fiber remodeling, and focal adhesion formation in 3D cell culture. *Biomaterials*, 154, 213–222. PMID: 29132046.

55. Chen, X., Liu, C., McDaniel, G., Zeng, O., Ali, J., Zhou, Y., Wang, X., Driscoll, T., Zeng, C., & Li, Y. (2024). Viscoelasticity of hyaluronic acid hydrogels regulates human pluripotent stem cell-derived spinal cord organoid patterning and vascularization. *Advanced Healthcare Materials*, 13, 2402199.

56. Nam, S., Stowers, R., Lou, J., Xia, Y., & Chaudhuri, O. (2019). Varying PEG density to control stress relaxation in alginate-PEG hydrogels for 3D cell culture studies. *Biomaterials*, 200, 15–24. PMID: 30716598.

57. Tang, S., Ma, H., Tu, H.-C., Wang, H.-R., Lin, P.-C., & Anseth, K. S. (2018). Adaptable fast relaxing boronate-based hydrogels for probing cell–matrix interactions. *Advanced Science*, 5(9), 1800638. PMID: 30250788.

58. McKinnon, D. D., Domaille, D. W., Cha, J. N., & Anseth, K. S. (2014). Biophysically defined and cytocompatible covalently adaptable networks as viscoelastic 3D cell culture systems. *Advanced Materials*, 26(6), 865–872. PMID: 24127293.

59. McKinnon, D. D., Domaille, D. W., Brown, T. E., Kyburz, K. A., Kiyotake, E., Cha, J. N., & Anseth, K. S. (2014). Measuring cellular forces using bis-aliphatic hydrazone crosslinked stress-relaxing hydrogels. *Soft Matter*, 10(46), 9230–9236. PMID: 25265090.

60. Sinha, S., Ayushman, M., Tong, X., & Yang, F. (2023). Dynamically crosslinked poly(ethylene-glycol) hydrogels reveal a critical role of viscoelasticity in modulating glioblastoma fates and drug responses in 3D. Advanced Healthcare Materials, 12(1), e2202147.

61. Skelton, M. L., Gentry, J. L., Astrab, L. R., Goedert, J. A., Earl, E. B., Pham, E. L., Bhat, T., & Caliari, S. R. (2024). Modular multiwell viscoelastic hydrogel platform for two- and three-dimensional cell culture applications. *ACS Biomaterials Science & Engineering*, 10(5), 3280–3292. PMID: 37873098.

62. Grad, E. M., Tunn, I., Voerman, D., de Léon, A. S., Hammink, R., & Blank, K. G. (2020). Influence of network topology on the viscoelastic properties of dynamically crosslinked hydrogels. *Frontiers in Chemistry*, 8, 536. PMID: 32719773.

63. Wang, K., Zhang, Y., Chen, T., Bai, L., Li, H., Tan, H., Liu, C., & Qu, X. (2023). Chain entanglement-driven tough, fatigue-resistant PEG-based injectable hydrogel adhesive for joint

skin wound healing. Composites Part B: Engineering, 266, 110991.

64. He, X., Hahn, P., Iacovelli, J., Wong, R., King, C., Bhisitkul, R., Massaro-Giordano, M., & Dunaief, J. L. (2007). Iron homeostasis and toxicity in retinal degeneration. Progress in Retinal and Eye Research, 26(6), 649–673.

65. Confalonieri, F., Ferraro, V., Barone, G., Di Maria, A., Petrovski, B. É., Vallejo Garcia, J. L., Randazzo, A., Vinciguerra, P., Lumi, X., & Petrovski, G. (2024). Outcomes in the treatment of subretinal macular hemorrhage secondary to age-related macular degeneration: A systematic review. Journal of Clinical Medicine, 13(2), 367.

66. Yang, S., Zhao, J., & Sun, X. (2016). Resistance to anti-VEGF therapy in neovascular age-related macular degeneration: A comprehensive review. *Drug Design, Development and Therapy, 10*, 1857–1867.

67. Monés, J., Garcia, M., Biarnés, M., Lakkaraju, A., & Ferraro, L. (2017). Drusen ooze: A novel hypothesis in geographic atrophy. *Ophthalmology Retina, 1*(6), 461–473.

68. Csaky, K. G., Patel, P. J., Sepah, Y. J., Birch, D. G., Do, D. V., Ip, M. S., Guymer, R. H., Luu, C. D., Gune, S., Lin, H., & Ferrara, D. (2019). Microperimetry for geographic atrophy secondary to age-related macular degeneration. *Survey of Ophthalmology, 64*(3), 353–364.

69. Pfeffer, B. A., & Fliesler, S. J. (2022). Reassessing the suitability of ARPE-19 cells as a valid model of native RPE biology. Experimental Eye Research, 219, 109046.

70. Mastrullo, V., Cathery, W., Velliou, E., Madeddu, P., & Campagnolo, P. (2020). Angiogenesis in tissue engineering: As nature intended? *Frontiers in Bioengineering and Biotechnology, 8*, 188.

71. Reddy, M. S. B., Ponnamma, D., Choudhary, R., & Sadasivuni, K. K. (2021). A comparative review of natural and synthetic biopolymer composite scaffolds. *Polymers, 13*(7), 1105.

72. Zhu, J., & Marchant, R. E. (2011). Design properties of hydrogel tissue-engineering scaffolds. *Expert Review of Medical Devices, 8*(5), 607–626.

73. Rosales, A. M., & Anseth, K. S. (2016). The design of reversible hydrogels to capture extracellular matrix dynamics. *Nature Reviews Materials, 1*, 15012.

74. Zhu, J. (2010). Bioactive modification of poly(ethylene glycol) hydrogels for tissue engineering. *Biomaterials, 31*(17), 4639–4656.

75. Terriac, L., Helesbeux, J.-J., Maugars, Y., Guicheux, J., Tibbitt, M. W., & Delplace, V. (2024). Boronate ester hydrogels for biomedical applications: Challenges and opportunities. Chemistry of Materials, 36(14), 6674–6695.

76. Zhang, Y., Lou, H., Yan, C., Zhang, Q., Wang, Y., & Zhang, Y. (2026). High entanglement in hydrogels: From polymer physics to robust mechanics. *Polymer Science & Technology, 2*(4), 222–247.

77. Läuger, J., & Stettin, H. (2016). Effects of instrument and fluid inertia in oscillatory shear in rotational rheometers. *Journal of Rheology, 60*(3), 393–406.

78. Sen, S., Dong, C., D'Aquino, A. I., Yu, A. C., & Appel, E. A. (2024). Biomimetic non-ergodic aging by dynamic-to-covalent transitions in physical hydrogels. ACS Applied Materials & Interfaces, 16(25), 32599–32610.

79. Li, J., & Mooney, D. J. (2016). Designing hydrogels for controlled drug delivery. *Nature Reviews Materials, 1*, 16071.

80. Drugs.com. (2026). *Macular degeneration: What you need to know*. Drugs.com.

81. Piskova, T., Kozyrina, A. N., & Di Russo, J. (2023). Mechanobiological implications of age-related remodelling in the outer retina. *Biomaterials Advances*, 147, 213343.

82. Fleckenstein, M., Keenan, T. D. L., Guymer, R. H., Chakravarthy, U., Schmitz-Valckenberg, S., Klaver, C. C., Wong, W. T., & Chew, E. Y. (2021). Age-related macular degeneration. *Nature Reviews Disease Primers*, 7(1), 31.

83. Vitreous Retina Macula Consultants of New York. (2024). Intravitreal injection. VRMNY.

84. Salehi-Had, H. (2024). Intravitreal injection for macular edema. Retina Associates of Southern California.

85. Med Learning Group. (2025). Pathophysiology of AMD. Vision RELIEF.

86. Jeyaraj, R., G, N., Kirby, G., Rajadas, J., Mosahebi, A., Seifalian, A. M., & Tan, A. (2015). Vascularisation in regenerative therapeutics and surgery. *Materials Science and Engineering: C*, 54, 225-238.

87. Stanford Artificial Retina Project. (2019). Research. Stanford Medicine.